National Library of Canada
Acquisitions and Bibliographic Services Branch
395 Wellington Street
Ottawa, Ontario
K1A 0N4

Bibliothèque nationale du Canada
Direction des acquisitions et des services bibliographiques
395, rue Wellington
Ottawa (Ontario)
K1A 0N4

Your file Votre référence

Our file Notre référence

NOTICE

The quality of this microform is heavily dependent upon the quality of the original thesis submitted for microfilming. Every effort has been made to ensure the highest quality of reproduction possible.

If pages are missing, contact the university which granted the degree.

Some pages may have indistinct print especially if the original pages were typed with a poor typewriter ribbon or if the university sent us an inferior photocopy.

AVIS

La qualité de cette microforme dépend grandement de la qualité de la thèse soumise au microfilmage. Nous avons tout fait pour assurer une qualité supérieure de reproduction.

S'il manque des pages, veuillez communiquer avec l'université qui a conféré le grade.

La qualité d'impression de certaines pages peut laisser à désirer, surtout si les pages originales ont été dactylographiées à l'aide d'un ruban usé ou si l'université nous a fait parvenir une photocopie de qualité inférieure.

Canada

ULTRASONIC THIN-WALLED TUBE WAVE DEVICES

Xing Li

A thesis

in

The Department

of

Physics

Presented in Partial Fulfillment of the Requirements
for the Degree of the Master of Science at
Concordia University
Montreal, Quebec, Canada

September 1994

ISBN 0-315-97671-3

Canada

ABSTRACT

Ultrasonic Thin-Walled Tube Devices

Xing Li

Ultrasonic devices employing thin-walled tubes for sensor considerations are theoretically and experimentally investigated. Similar to ultrasonic plate wave sensors these configurations have advantages of separating the sensing medium from the sensor electronics and of high mass sensitivity for several modes provided that the tube wall thickness h is very thin. Furthermore, the inner side of the tube can be used as the chamber or flow channel of the gases or liquid to be monitored.

In order to achieve an integrated sensor configuration, a sol-gel process for the fabrication of thin piezoelectric lead zirconate titanate (PZT) films coated coaxially on stainless steel tubes is developed. PZT film thickness up to several microns and coating length more than several centimeters have been achieved. Interdigital transducers (IDT) which excite the ultrasonic waves are fabricated as the transmitter and receiver on the curved tube surfaces. Along the axial direction, delay line configurations are adopted to measure the velocity and phase change of the acoustic modes. Along the circumferential direction a resonator or delay line geometry is made with one IDT. Experimental measurements with good signal to noise ratio at frequencies between 1 and 8 MHz are presented. Effect of liquid loading in the tube device is also investigated.

The wave propagation characteristics in both the axial and circumferential directions of the cylindrical shells, as well as the mass sensitivity of the thin-walled tube wave devices, are theoretically analyzed. Explicit formulas for the mass sensitivities of several modes such as the lowest axially symmetric mode and torsional mode were derived and compared with those of the

bulk, plate and thin rod acoustic wave sensor devices. The high mass sensitivity can be achieved by using thin wall (small h) tubes and it makes these devices excellent sensor candidates.

ACKNOWLEDGMENT

I am very grateful to my supervisor Professor J.D.N. Cheeke, for his guidance and support in my study. It was he who brought me into the field of ultrasonics. I appreciate the financial support from the Institute of Chemical Science and Technology of Canada to part of this project, and that from the Concordia University Graduate Fellowship to my M.Sc. programme.

My special gratitude is expressed to Dr. C.K. Jen. His valuable advice, efficient assistance, consistent encouragement and critical comments were very helpful in my research and very crucial for me to complete this project.

I wish to thank Prof. Z. Wang for the valuable discussions in the theoretical analysis. My appreciation is extended to Dr. M. Viens for his assistance in my experiments and drawing of several figures used in this thesis. I also acknowledge Dr. G. Yi of Queen's University, for his instruction in my learning of the PZT sol-gel process, which made the integrated tube devices possible, and Professor M. Sayer for kindly allowing me to use some facilities in his laboratory at Queen's University.

Many thanks are given to my colleagues S. Beaudin, M. Dan, P. Ji, N. Tashtoush, T. Laurent and G. Quirion for their friendly help and cooperation during the course of the study. Assistance from G. Thompson and L. Chapman are also appreciated.

I am deeply indebted to my wife and daughter for their love and support, without which I could not have finished this work. A final thank is dedicated to my parents who have always encouraged me.

TABLE OF CONTENTS

LIST OF FIGURES

LIST OF TABLES

CHAPTER 1: INTRODUCTION

There has been growing interest in the development of integrated acoustic sensors in the past two decades. Most of them are based on bulk acoustic waves (BAW) [1-14], surface acoustic waves (SAW) including shear-horizontal and Love types [15-41], plate acoustic waves including Lamb and shear-horizontal types [42-54], and most recently thin rod acoustic waves [55-60]. These sensors are used for chemical sensing in either gases or liquids, to determine concentrations of certain chemical and biological substances [6,7,9,19,12,17,18,20,24-28,35,39,40,51,60,61], as well as for physical property monitoring such as film thickness [1-4], temperature [15,18,34], pressure [15,16,30], viscosity [8,13,16,34,36,52,54], acceleration [29], and voltage [21], etc. Fig.1.1 briefly illustrates the geometrical configurations of the above sensors employing four different types of acoustic waves.

When additional mass is loaded onto the sensing surface of a device, it causes changes in the acoustic properties. In an acoustic delay line, a perturbation leads to a change of the wave velocity and thus a change of the time for the waves traveling from the transmitter to the receiver. In a resonator, the resonant frequency shifts from the unloaded resonant frequency, due to the loaded mass. A sensor coated with chemical or biological selective layer(s) may be able to bind particular particles of interest onto its surface. By measuring and analyzing the change of the acoustic parameters due to the mass loading, the so called gravimetric effect, information about the concentration of the attached substances in the medium (gas or liquid) may be obtained. A review article [61] has outlined several basic requirements of such chemically-selective coatings. In order to reduce the sensor noise caused by environmental fluctuations such as temperature and pressure, in general a dual-channel configuration [19,22] was used.

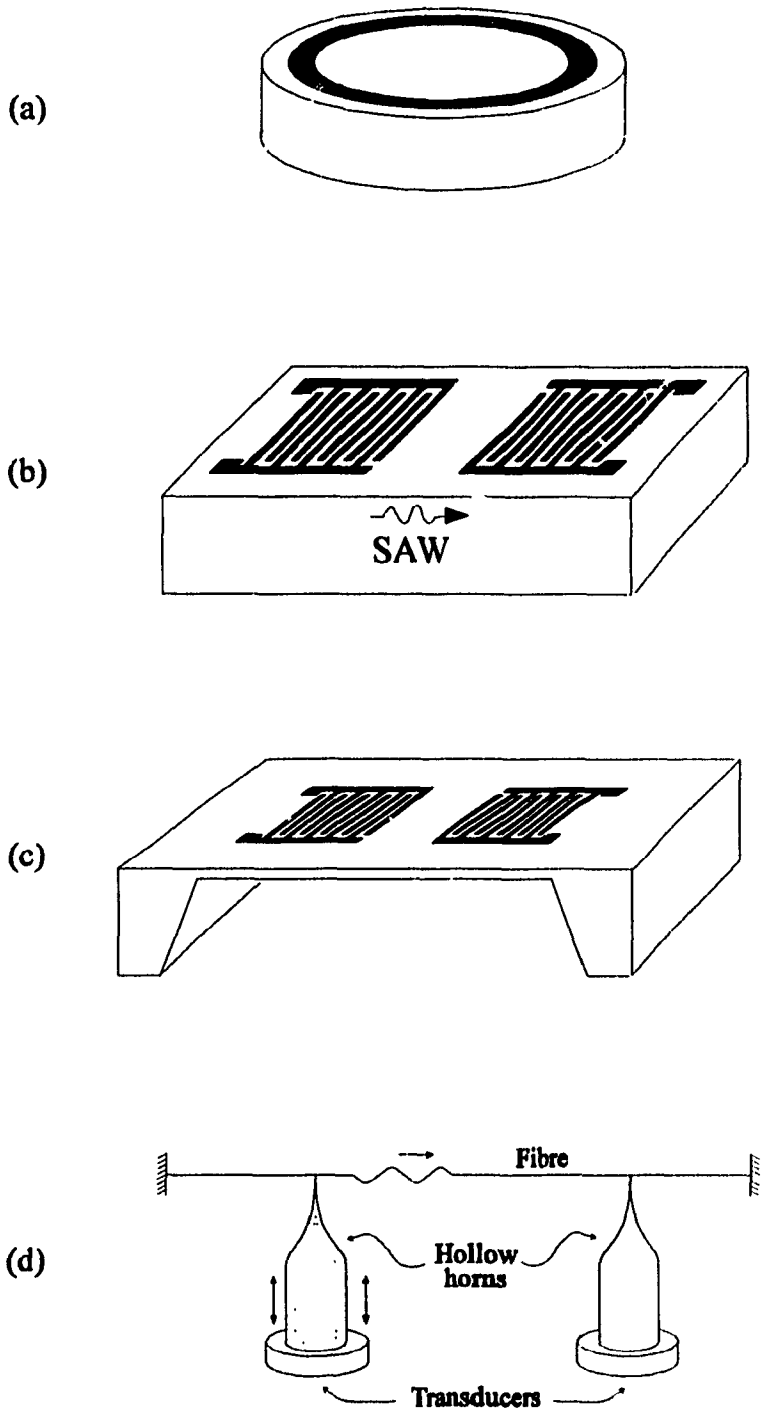

Figure 1.1 Four different geometries (a) bulk, (b) surface, (c) plate, and (d) fibre acoustic wave devices

Many recent studies have been reported on membranes and fibres, which have considerably higher sensitivity than traditional BAW and SAW devices [46-58]. In general, the mass sensitivity is inversely proportional to the mass per unit area of a characteristic layer in the thickness direction of the device substrate. Physically this layer is the active region of the device that stores elastic energy and is perturbed by changes of surface mass. For the BAW and SAW sensors the thickness of this layer is approximately the operating wave length, and for the plate and thin rod devices it is the plate thickness or the rod diameter. To increase the sensitivity of the BAW or SAW sensors, the wavelength must be decreased, or equivalently the frequency must be increased. By using very thin plates or fibres, the sensitivity can be substantially increased independent of the wavelength and thus the wave velocity. In addition, for a given acoustic wavelength, in the lowest antisymmetric (A_0) mode the phase velocity decreases as the plate thickness or the rod diameter reduces. Therefore, these sensors can work at a very low frequency and velocity with a high sensitivity. Furthermore, the sensitivity of a lowest symmetric (S_0) or shear-horizontal (SH_0) plate acoustic wave sensor and that of a lowest order extensional or torsional fibre acoustic wave sensor are also inversely proportional to their thickness (or diameter), when the product of the frequency and the thickness (or diameter) is very small [50-64]. In addition to the high sensitivities, thin plate acoustic wave devices offer a significant advantage in that the sensing region and the device electronics are separated by the thin plate [42,45-48,50,51].

However, for the sensing application in gases or liquids, the plate wave (also BAW and SAW) sensors require containers for the gases or liquids to be monitored, as shown in Fig.1.2. Often, the construction of these containers need special attention and sometimes makes the device impractical for use. The development of tube sensors comes from the consideration of an improvement in this respect.

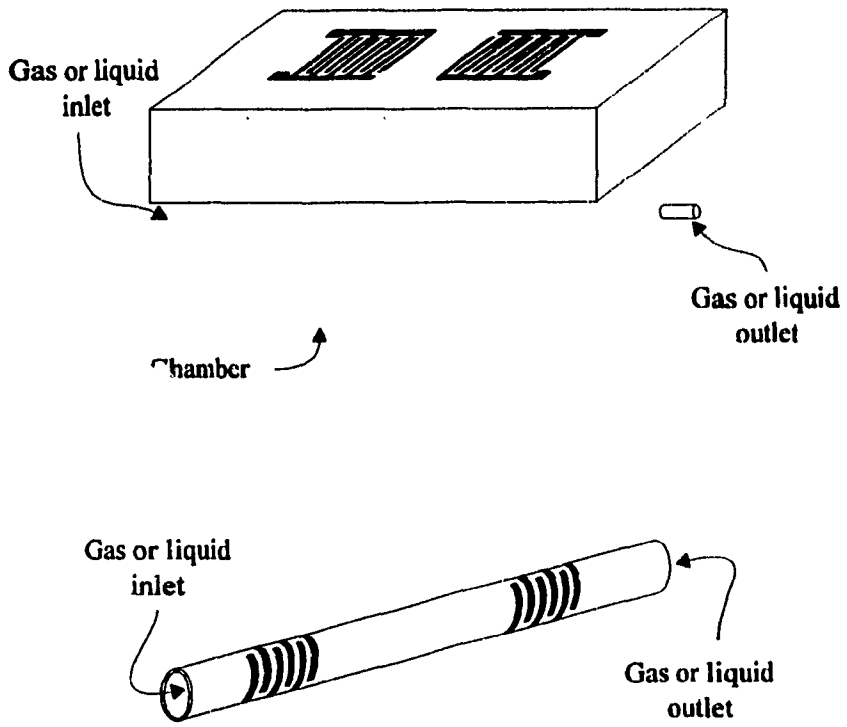

Figure 1.2 Comparison between plate and tube wave devices in the aspect of the chamber containing gas or liquid to be monitored

As in the case of the thin plate, when the tube wall is thin enough, the wave energy can be present on both its inner and outer sides, allowing one of its sides, say the inner one, to be used as the active sensing surface and the other side to be equipped with device electronics. It can be expected that properties of the wave propagating in a tube whose wall thickness is very small compared to its diameter are very similar in many ways to those of a thin membrane. Thus a thin-walled tube, with many advantages of the thin plate devices, offers a unique geometrical structure where, for instance, the inner side is naturally used as the container for the gases or the liquids to be sensed, as shown in Fig.1.2. A tube delay-line sensor, which is very similar to a plate wave delay

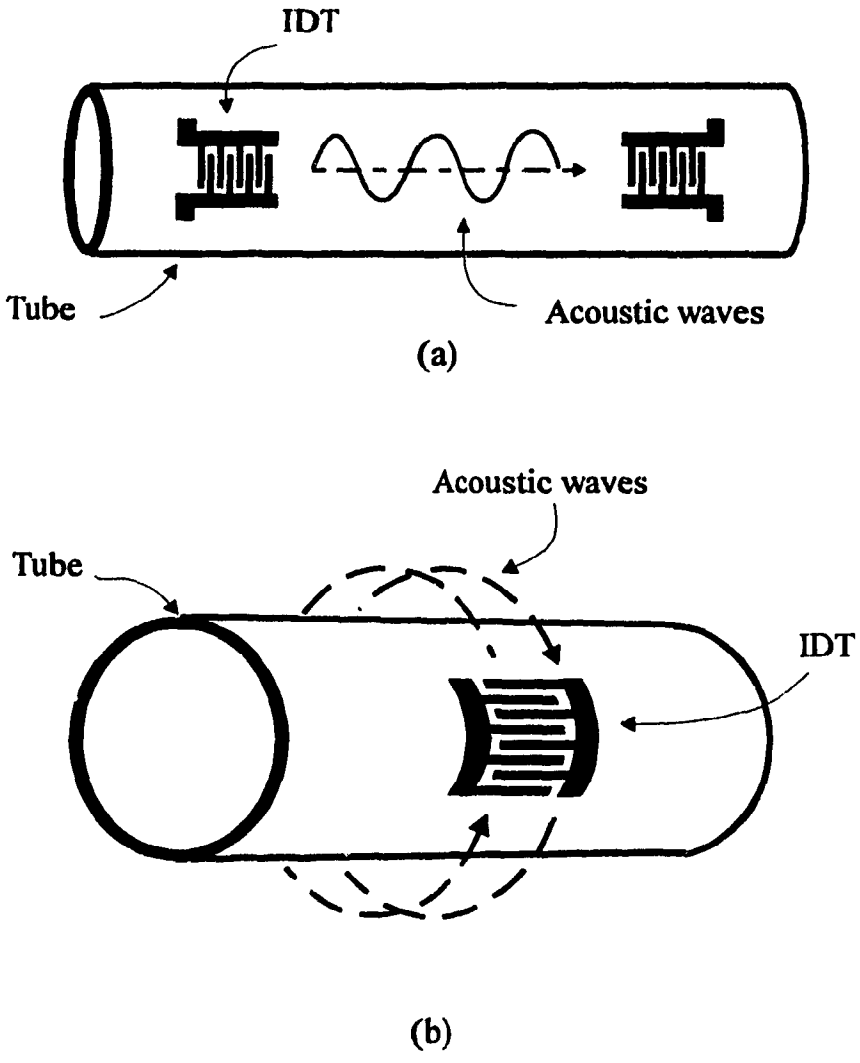

Figure 1.3 Two geometries of tube devices: (a) axial wave delay line, and (b) circumferential wave delay line or resonator.

line, is illustrated in Fig.1.3 (a). In addition to the delay-line configuration, the tube wave devices can be also used in a resonator structure. Furthermore, along the circumferential direction of the tube it is possible that only one transducer is used, and waves excited in both directions have the same contribution and travel along the circumference without reflection (See Fig.1.3 (b)).

While some approaches and technologies for SAW and plate wave sensors may readily be employed in the tube sensors, such as interdigital transducers (IDT) and their fabrication, theoretical analysis for tube waves and actual techniques for fabricating the tube devices are indispensable.

Problems of wave propagation in a hollow cylindrical structure are in principle more complicated than in the planar structure. Although interest in the study of elastic waves in cylindrical structures goes back more than one hundred years [62], it has been only in recent decades that exact solutions for elastic waves in thick shells were obtained and varied approximate theories were developed for thin shells, only a few of which [63-71,77,78] are quoted here. Their results were displayed in terms of dispersion curves, displacement and stress distributions for infinite as well as finite shells either in a vacuum or in an acoustic medium (water). Experimental results were also obtained and compared with the theories [73-76]. However, while the wave propagation in the axial direction has been extensively studied, only a few reports on that along the circumferential direction are found in the literature [77][78] (those on circumferential surface waves are not included) and the theories given were not complete.

In this thesis a general analysis of the waves in a cylindrical shell will be outlined, including both axial and circumferential directions, which provides a guideline for the selection of proper modes for practical device considerations. Special attention is devoted to circumferential modes.

Technologically, one important concern is how to achieve an integrated tube wave device which is of practical interest. A practical approach is to coat piezoelectric layers onto the tube surface, as shown in Fig.1.4, which converts the electrical and energy and energies from one to another. In general, piezoelectric thin films such as ZnO and AlN

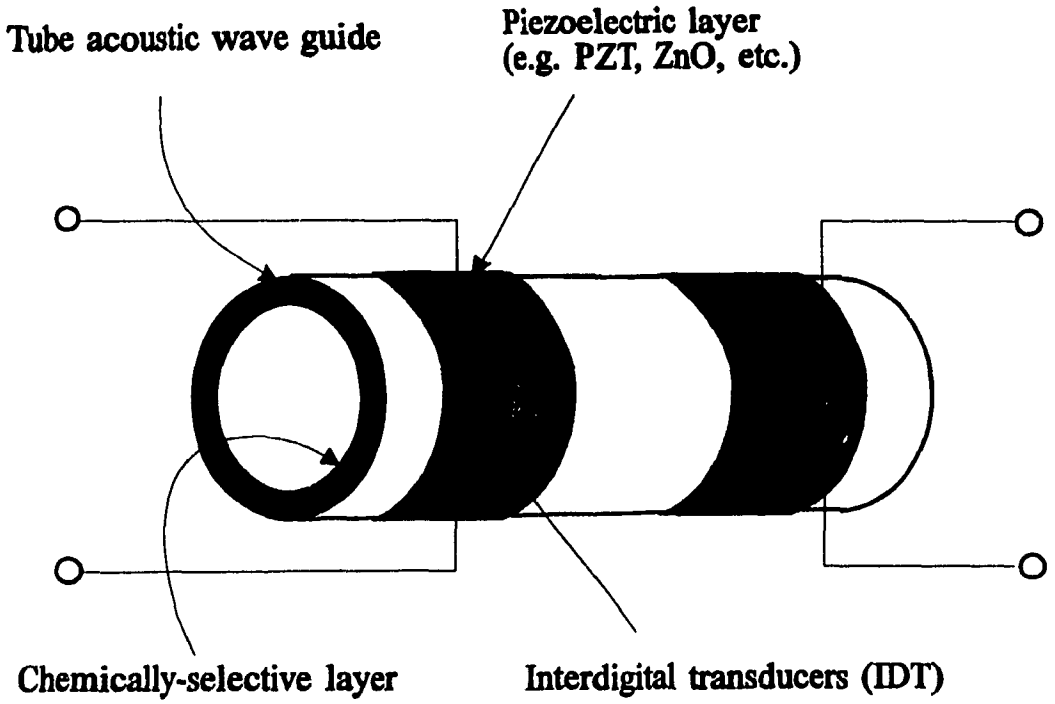

Figure 1.4 Structure of a typical tube sensor

fabricated by conventional vacuum sputtering techniques, which have been used for planar substrates in SAW or membrane devices, are difficult to coat on surfaces with large curvatures, metallic substrates and substrates with a long coating length. Lead zirconate titanate (PZT) ceramics, have been widely used as a class of piezoelectric and acoustic transducer materials because of their large piezoelectric coupling coefficients [80]. Up to 1987, the fabrication of PZT films had been reported primarily using techniques such as rf sputtering, electron beam evaporation and ion beam deposition. More recently, pulse laser deposition has been explored [81]. These physical deposition techniques have the common feature that it is necessary to deposit the films in high vacuum and to sputter or evaporate materials from a multicomponent material source. This implies that a complex set of conditions has to be met to obtain good quality films. In recent years, fabrication of PZT films by the chemical sol-gel method [82-90] has become attractive, because of its

advantages such as easier fabrication of large areas and on complex shapes [88,89], suitability for metallic substrates [88], low cost, short fabrication cycle, etc.

Once tubes coated with piezoelectric layers are available, technologies used in SAW and thin plate devices for fabricating the interdigital transducers (IDT), which excite acoustic waves in the piezoelectric layer and reconvert them into electrical signals, can be then adopted here. However, special procedures must be developed since for the tube devices the IDTs are to be made on curved surfaces rather than on flat ones.

In this thesis we introduce and develop ultrasonic devices employing thin-wall tubes for sensor considerations, which is an extension of the previous works on thin membrane and fibre acoustic sensors. Related theories are studied and applied to this subject.

Chapter 2 gives the fundamentals. In Chapter 2.1 a general description is introduced of waves propagating in cylindrical shells and particular discussions are given on circumferential waves. Gravimetric sensitivities of tube sensors derived using perturbation theory are discussed in Chapter 2.2.

Chapter 3 presents detailed descriptions of the experimental procedures for thin-walled tube fabrication, PZT film coating and IDT transducers making.

In Chapter 4 we show experimental results of the tubes wave devices, and evaluate their sensing features. Concluding remarks and comments on further development of the sensors are given in Chapter 5.

CHAPTER 2 : THEORIES

2.1 ELASTIC WAVES PROPAGATING IN CYLINDRICAL SHELLS

The propagation of free harmonic waves along a hollow cylinder of infinite extent was studied by *Gasiz* [67, 68] and many others (not quoted here), within the framework of the linear theory of elasticity. The waves considered were coherently propagating along axial direction in sinusoidal function form, and the acoustic fields in the circumferential direction were *stationary* and periodic. In our sensing application involving circumferential modes, the *traveling waves* rather than the stationary ones are of interest. The three-dimensional theory given in [68] is reviewed here first, and then its extension will be developed in section 2.1.1, to accommodate the propagating circumferential waves.

Consider a concentrical hollow cylinder with finite thickness $h = b\text{-}a$, where a and b are the inner and outer radii, respectively (Fig. 2.1).

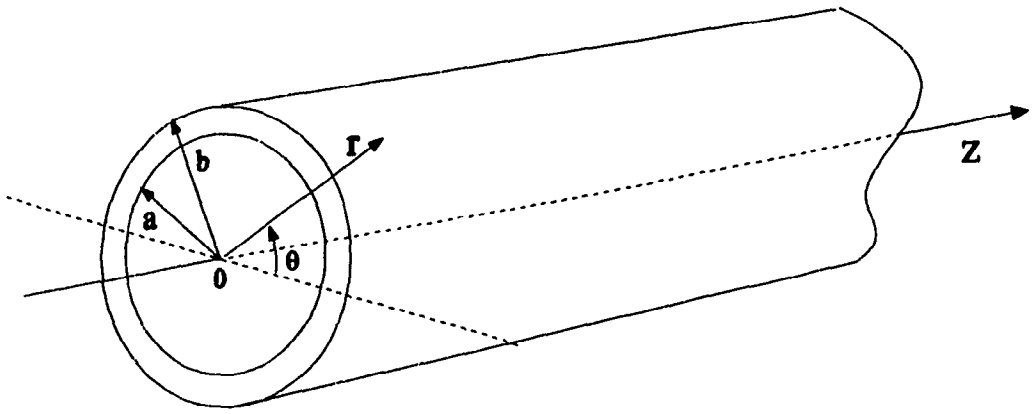

Figure 2.1. Cylindrical shell and the co-ordinate system

The equations of motion for an isotropic elastic medium are, in invariant form,

$$\nabla^2 \mathbf{u} + (1+\frac{\lambda}{\mu})\nabla\nabla\cdot\mathbf{u} = \frac{\rho}{\mu}\frac{\partial^2 \mathbf{u}}{\partial t^2} \tag{2.1}$$

where $\mathbf{u}$ is the displacement vector, ρ is the density, λ and μ are the Lame's constant, and ∇^2 is the Laplace's operator. The displacement $\mathbf{u}$ is expressed in terms of a dilatational scalar potential φ and an equivoluminal vector potential $\boldsymbol{\psi}$ according to

$$\mathbf{u} = \nabla\varphi + \nabla\times\boldsymbol{\psi}, \tag{2.2}$$

with

$$\nabla\cdot\boldsymbol{\psi} = 0. \tag{2.3}$$

The displacement equations of motion are satisfied if the potentials satisfy the wave equations

$$\begin{aligned} \nabla^2\varphi &= \frac{1}{V_L^2}\frac{\partial^2\varphi}{\partial t^2}; \\ \nabla^2\boldsymbol{\psi} &= \frac{1}{V_S^2}\frac{\partial^2\boldsymbol{\psi}}{\partial t^2}, \end{aligned} \tag{2.4}$$

where V_L and V_S represent the longitudinal and shear wave velocities in this bulk material, respectively, and given by

$$\begin{aligned} V_L^2 &= (\lambda+2\mu)/\rho; \\ V_S^2 &= \mu/\rho. \end{aligned} \tag{2.5}$$

In detail, the Helmholtz equations (2.4) can be expressed in cylindrical coordinates by

$$
\begin{aligned}
&\left(\nabla^2+\omega^2/V_L^2\right)\phi=0;\\
&\left(\nabla^2+\omega^2/V_S^2\right)\psi_z=0;\\
&\left(\nabla^2-1/r^2+\omega^2/V_S^2\right)\psi_r-(2/r^2)(\partial\psi_\theta/\partial\theta)=0;\\
&\left(\nabla^2-1/r^2+\omega^2/V_S^2\right)\psi_\theta+(2/r^2)(\partial\psi_r/\partial\theta)=0.
\end{aligned}
\tag{2.6}
$$

Let the potentials be of the form

$$
\begin{aligned}
\varphi &= f(r)\cdot\cos(n\theta)\cdot\exp[j(\gamma z+\omega t)];\\
\psi_r &= g_r(r)\cdot\sin(n\theta)\cdot\exp[j(\gamma z+\omega t)];\\
\psi_\theta &= g_\theta(r)\cdot\cos(n\theta)\cdot\exp[j(\gamma z+\omega t)];\\
\psi_z &= g_z(r)\cdot\sin(n\theta)\cdot\exp[j(\gamma z+\omega t)],
\end{aligned}
\tag{2.7}
$$

where γ is the axial propagation constant. The waves propagate in the positive axial direction, and around the circumference the waves are stationarily distributed in an arbitrary numbe: of waves n. By substituting Eqs.(2.7) into Eq.(2.6), one obtains

$$\frac{\partial^2 f(r)}{\partial r^2}+\frac{1}{r}\cdot\frac{\partial f(r)}{\partial r}+\left[\alpha^2-\frac{n^2}{r^2}\right]f(r)=0; \tag{2.8-a}$$

$$\frac{\partial^2 g_z(r)}{\partial r^2}+\frac{1}{r}\cdot\frac{\partial g_z(r)}{\partial r}+\left[\beta^2-\frac{n^2}{r^2}\right]g_z(r)=0; \tag{2.8-b}$$

$$\frac{\partial^2 g_r(r)}{\partial r^2}+\frac{1}{r}\cdot\frac{\partial g_r(r)}{\partial r}+\left[\beta^2-\frac{n^2+1}{r^2}\right]g_r(r)+\frac{2n}{r^2}\cdot g_\theta=0; \tag{2.8-c}$$

$$\frac{\partial^2 g_\theta(r)}{\partial r^2}+\frac{1}{r}\cdot\frac{\partial g_\theta(r)}{\partial r}+\left[\beta^2-\frac{n^2+1}{r^2}\right]g_\theta(r)+\frac{2n}{r^2}\cdot g_r=0, \tag{2.8-d}$$

where a and b are the radial component of the longitudinal and shear wave vectors, respectively, which are given as

$$\alpha^2 = \omega^2 / V_L^2 - \gamma^2;$$
$$\beta^2 = \omega^2 / V_S^2 - \gamma^2. \tag{2.9}$$

Eqs. (2.8-a, 2.8-b) are the standard Bessel's equations and their solutions are the Bessel functions with arguments αr and βr. Considering the case $\alpha^2 > 0$ and $\beta^2 > 0$, the general solutions can be given by,

$$f = A \cdot J_n(\alpha r) + B \cdot Y_n(\alpha r);$$
$$g_3 = g_z = C_2 \cdot J_n(\beta r) + D_2 \cdot Y_n(\beta r), \tag{2.10}$$

where, J_n and Y_n are the first and second Bessel's functions of nth order, respectively. Subtracting Eq.(2.8-d) from Eq.(2.8-c) gives

$$\left[\frac{\partial^2}{\partial r^2} + \frac{1}{r}\cdot\frac{\partial}{\partial r} + \beta^2 - \frac{(n+1)^2}{r^2}\right]\cdot[g_r(r) - g_\theta(r)] = 0, \tag{2.11.1}$$

and adding Eq.(2.8-c) to Eq.(2.8-d) yields

$$\left[\frac{\partial^2}{\partial r^2} + \frac{1}{r}\cdot\frac{\partial}{\partial r} + \beta^2 - \frac{(n-1)^2}{r^2}\right]\cdot[g_r(r) + g_\theta(r)] = 0. \tag{2.11-2}$$

The solutions of Eqs. (2.11-1) and(2.11-2) can then be given by

$$g_1 = (1/2)(g_r - g_\theta) = C_1 \cdot J_{n+1}(\beta r) + D_1 \cdot Y_{n+1}(\beta r);$$
$$g_2 = (1/2)(g_r + g_\theta) = A_2 \cdot J_{n-1}(\beta r) + B_2 \cdot Y_{n-1}(\beta r). \tag{2.12}$$

The property of the *gauge invariance* can now be utilized in order to eliminate two of the integration constants of Eqs.(2.12). Owing to this property, any one of the three potential components of g_i $(i=1,2,3)$ can be set to zero, without loss of the generality of solution. Physically, this implies that the displacement field corresponding to equivoluminal potential g_i can also be derived by a combination of the other two equivoluminal potentials. Setting $g_2 = 0$, we have

$$g_r = -g_\theta = g_1 \tag{2.13}$$

The resulting displacements are then given by

$$\begin{aligned} u_r &= \left[f' + (n/r)g_3 + j\gamma\, g_1\right] \cdot \cos(n\theta) \cdot \exp[j(\gamma z + \omega t)]; \\ u_\theta &= \left[-(n/r)f - g'_3 + j\gamma\, g_1\right] \cdot \sin(n\theta) \cdot \exp[j(\gamma z + \omega t)]; \\ u_z &= \left[j\gamma f - g'_1 - (n+1)(g_1/r)\right] \cdot \cos(n\theta) \cdot \exp[j(\gamma z + \omega t)], \end{aligned} \tag{2.14}$$

where primes denotes differentiation with respect to r.

The stress components are

$$\begin{aligned} T_{rr} &= \sigma_{rr} \cdot \cos(n\theta) \cdot e^{j(\gamma z + \omega t)}; \\ T_{r\theta} &= \sigma_{r\theta} \cdot \sin(n\theta) \cdot e^{j(\gamma z + \omega t)}; \\ T_{rz} &= \sigma_{rz} \cdot \cos(n\theta) \cdot e^{j(\gamma z + \omega t)}, \end{aligned} \tag{2.15}$$

where the distributions of the stresses are given by

$$\begin{aligned} \sigma_{rr} &= -\lambda\,(\alpha^2 + \gamma^2) f + 2\mu\left[f'' + j\gamma\, g'_1 + \frac{n}{r}\left(g'_3 - \frac{g_3}{r}\right)\right]; \\ \sigma_{r\theta}/\mu &= -\frac{2n}{r}\left(f' - \frac{f}{r}\right) - j\gamma \cdot \left(\frac{n+1}{r} \cdot g_1 - g'_1\right) - \left(2g_3'' - \beta^2 g_3\right); \\ \sigma_{rz}/\mu &= 2j\gamma \cdot f' - \frac{n}{r} g_1' - \left(\frac{n(n+1)}{r^2} - \beta^2 + \gamma^2\right) \cdot g_1 + j\gamma \cdot \frac{n}{r} \cdot g_3 . \end{aligned} \tag{2.16}$$

The boundary conditions, for free motion, are

$$\sigma_{rr} = \sigma_{r\theta} = \sigma_{rz} = 0, \quad \text{at } r = a \text{ and } r = b \tag{2.17}$$

The frequency equations result from substituting Eq. (2.16) in (2.17), with six constants A, B, C, D, E, and F appearing in each of the six boundary condition equations. A necessary and sufficient condition for the existence of a nontrivial solution is that the determinant of coefficients must vanish, i.e.

$$\begin{vmatrix} \Gamma_{11} & \Gamma_{12} & \Gamma_{13} & \Gamma_{14} & \Gamma_{15} & \Gamma_{16} \\ \Gamma_{21} & \Gamma_{22} & \Gamma_{23} & \Gamma_{24} & \Gamma_{25} & \Gamma_{26} \\ \Gamma_{31} & \Gamma_{32} & \Gamma_{33} & \Gamma_{34} & \Gamma_{35} & \Gamma_{36} \\ \Gamma_{41} & \Gamma_{42} & \Gamma_{43} & \Gamma_{44} & \Gamma_{45} & \Gamma_{46} \\ \Gamma_{51} & \Gamma_{52} & \Gamma_{53} & \Gamma_{54} & \Gamma_{55} & \Gamma_{56} \\ \Gamma_{61} & \Gamma_{62} & \Gamma_{63} & \Gamma_{64} & \Gamma_{65} & \Gamma_{66} \end{vmatrix} = 0 \tag{2.18}$$

where the elements are given by

$$\Gamma_{11} = \left[2k_L^2 - k_S^2\right] \cdot J_n(x_1) + 2\alpha^2 \cdot J''_n(x_1)$$

$$\Gamma_{12} = \left[2k_L^2 - k_S^2\right] \cdot Y_n(x_1) + 2\alpha^2 \cdot Y''_n(x_1)$$

$$\Gamma_{13} = 2j\gamma\beta \cdot J'_{n+1}(y_1)$$

$$\Gamma_{14} = 2j\gamma\beta \cdot Y'_{n+1}(y_1)$$

$$\Gamma_{15} = \frac{2n}{y_1}\beta^2 \cdot \left[J_n'(y_1) - \frac{J_n(y_1)}{y_1}\right]$$

$$\Gamma_{16} = \frac{2n}{y_1}\beta^2 \cdot \left[Y_n'(y_1) - \frac{Y_n(y_1)}{y_1}\right]$$

$$\Gamma_{21} = \left[2k_L^2 - k_S^2\right] \cdot J_n(x_2) + 2\alpha^2 \cdot J''_n(x_2)$$
$$\Gamma_{22} = \left[2k_L^2 - k_S^2\right] \cdot Y_n(x_2) + 2\alpha^2 \cdot Y''_n(x_2)$$
$$\Gamma_{23} = 2j\gamma\beta \cdot J'_{n+1}(y_2)$$
$$\Gamma_{24} = 2j\gamma\beta \cdot Y'_{n+1}(y_2)$$
$$\Gamma_{25} = \frac{2n}{y_2}\beta^2 \cdot \left[J_n'(y_2) - \frac{J_n(y_2)}{y_2}\right]$$
$$\Gamma_{26} = \frac{2n}{y_2}\beta^2 \cdot \left[Y_n'(y_2) - \frac{Y_n(y_2)}{y_2}\right]$$

$$\Gamma_{31} = \frac{-2n\alpha^2}{x_1} \cdot \left[J_n'(x_1) - \frac{J_n(x_1)}{x_1}\right]$$
$$\Gamma_{32} = \frac{-2n\alpha^2}{x_1} \cdot \left[Y_n'(x_1) - \frac{Y_n(x_1)}{x_1}\right]$$
$$\Gamma_{33} = j\gamma\beta \cdot \left[J'_{n+1}(y_1) - \frac{n+1}{y_1} J_{n+1}(y_1)\right]$$
$$\Gamma_{34} = j\gamma\beta \cdot \left[Y'_{n+1}(y_1) - \frac{n+1}{y_1} Y_{n+1}(y_1)\right]$$
$$\Gamma_{35} = \beta^2 \cdot \left[J_n(y_1) - 2 \cdot J''_n(y_1)\right]$$
$$\Gamma_{36} = \beta^2 \cdot \left[Y_n(y_1) - 2 \cdot Y''_n(y_1)\right]$$

(2.19)

$$\Gamma_{41} = \frac{-2n\alpha^2}{x_2} \cdot \left[J_n'(x_2) - \frac{J_n(x_2)}{x_2}\right]$$
$$\Gamma_{42} = \frac{-2n\alpha^2}{x_2} \cdot \left[Y_n'(x_2) - \frac{Y_n(x_2)}{x_2}\right]$$
$$\Gamma_{43} = j\gamma\beta \cdot \left[J'_{n+1}(y_2) - \frac{n+1}{y_2} J_{n+1}(y_2)\right]$$
$$\Gamma_{44} = j\gamma\beta \cdot \left[Y'_{n+1}(y_2) - \frac{n+1}{y_2} Y_{n+1}(y_2)\right]$$
$$\Gamma_{45} = \beta^2 \cdot \left[J_n(y_2) - 2 \cdot J''_n(y_2)\right]$$
$$\Gamma_{46} = \beta^2 \cdot \left[Y_n(y_2) - 2 \cdot Y''_n(y_2)\right]$$

$$\Gamma_{51} = 2j\gamma\alpha \cdot J_n'(x_1)$$
$$\Gamma_{52} = 2j\gamma\alpha \cdot Y_n'(x_1)$$
$$\Gamma_{53} = -\frac{n\beta^2}{y_1} \cdot J'_{n+1}(y_1) - \left[\frac{n(n+1)\beta^2}{y_1^2} - \beta^2 + \gamma^2\right] \cdot J_{n+1}(y_1)$$
$$\Gamma_{54} = -\frac{n\beta^2}{y_1} \cdot Y'_{n+1}(y_1) - \left[\frac{n(n+1)\beta^2}{y_1^2} - \beta^2 + \gamma^2\right] \cdot Y_{n+1}(y_1)$$
$$\Gamma_{55} = \frac{j\gamma\beta n}{y_1} \cdot J_n(y_1)$$
$$\Gamma_{56} = \frac{j\gamma\beta n}{y_1} \cdot Y_n(y_1)$$
$$\Gamma_{61} = 2j\gamma\alpha \cdot J_n'(x_2)$$
$$\Gamma_{62} = 2j\gamma\alpha \cdot Y_n'(x_2)$$
$$\Gamma_{63} = -\frac{n\beta^2}{y_2} \cdot J'_{n+1}(y_2) - \left[\frac{n(n+1)\beta^2}{y_2^2} - \beta^2 + \gamma^2\right] \cdot J_{n+1}(y_2)$$
$$\Gamma_{64} = -\frac{n\beta^2}{y_2} \cdot Y'_{n+1}(y_2) - \left[\frac{n(n+1)\beta^2}{y_2^2} - \beta^2 + \gamma^2\right] \cdot Y_{n+1}(y_2)$$
$$\Gamma_{65} = \frac{j\gamma\beta n}{y_2} \cdot J_n(y_2)$$
$$\Gamma_{66} = \frac{j\gamma\beta n}{y_2} \cdot Y_n(y_2)$$

where $x_1 = \alpha a$, $x_2 = \beta a$, $y_1 = \alpha b$ and $y_2 = \beta b$.

A. Circumferential modes - motion independent of z

Motion independent of z occurs when $\gamma = 0$, which corresponds to the cut-off condition, or the waves around the circumference. The determinant of coefficients reduces to

$$\begin{vmatrix} \Gamma_{11} & \Gamma_{12} & 0 & 0 & \Gamma_{15} & \Gamma_{16} \\ \Gamma_{21} & \Gamma_{22} & 0 & 0 & \Gamma_{25} & \Gamma_{26} \\ \Gamma_{31} & \Gamma_{32} & 0 & 0 & \Gamma_{35} & \Gamma_{36} \\ \Gamma_{41} & \Gamma_{42} & 0 & 0 & \Gamma_{45} & \Gamma_{46} \\ 0 & 0 & \Gamma_{53} & \Gamma_{54} & 0 & 0 \\ 0 & 0 & \Gamma_{63} & \Gamma_{64} & 0 & 0 \end{vmatrix} \tag{2.20}$$

$$= \begin{vmatrix} \Gamma_{11} & \Gamma_{12} & \Gamma_{15} & \Gamma_{16} \\ \Gamma_{21} & \Gamma_{22} & \Gamma_{25} & \Gamma_{26} \\ \Gamma_{31} & \Gamma_{32} & \Gamma_{35} & \Gamma_{36} \\ \Gamma_{41} & \Gamma_{42} & \Gamma_{45} & \Gamma_{46} \end{vmatrix} \cdot \begin{vmatrix} \Gamma_{53} & \Gamma_{54} \\ \Gamma_{63} & \Gamma_{64} \end{vmatrix} = \delta_1 \cdot \delta_2$$

Eq. (2.18) is satisfied if either

$$\delta_1 = \begin{vmatrix} \Gamma_{11} & \Gamma_{12} & \Gamma_{15} & \Gamma_{16} \\ \Gamma_{21} & \Gamma_{22} & \Gamma_{25} & \Gamma_{26} \\ \Gamma_{31} & \Gamma_{32} & \Gamma_{35} & \Gamma_{36} \\ \Gamma_{41} & \Gamma_{42} & \Gamma_{45} & \Gamma_{46} \end{vmatrix} = 0 \quad \text{or} \quad \delta_2 = \begin{vmatrix} \Gamma_{53} & \Gamma_{54} \\ \Gamma_{63} & \Gamma_{64} \end{vmatrix} = 0 \tag{2.21}$$

For $\delta_1 = 0$, set $C = 0, D = 0$

The displacements are then

$$\begin{aligned} u_r &= \left[f' + (n/r)g_3\right] \cdot \cos(n\theta) \cdot e^{j\omega t}, \\ u_\theta &= \left[-(n/r)f - g'_3\right] \cdot \sin(n\theta) \cdot e^{j\omega t}, \\ u_z &= 0 \end{aligned} \tag{2.22}$$

We can see that the waves are independent of z, and have both the radial and the angular components, which correspond to the sagittal-plane waves in the plate case. The dispersion relation in these circumferential modes is determined by solving $\delta_1 = 0$.

For $\delta_2 = 0$, setting $A = B = E = F = 0 \rightarrow f = g_3 = 0$,

the displacements becomes

$$\begin{aligned} u_r(r) &= 0 \\ u_\theta(r) &= 0 \\ u_z(r) &= [-g'_1 - (n+1)(g_1/r)] \cdot \cos(n\theta) \cdot e^{j\omega t} \end{aligned} \tag{2.23}$$

and only one component - the *longitudinal shear* [67,68]component exists, which corresponds to the *shear-horizontal* (*SH*) polarization in the flat plate case. Equation $\delta_2 = 0$ defines the dispersion relation of this type of modes.

B. Axial symmetric modes - motion independent of θ

In the case of $n = 0$, the motion is independent of θ and the acoustic fields around the circumference are uniform. These modes are referred to as axially symmetric modes. The waves with only circumferential displacement is referred to as torsional modes, and those with the axial-radial polarizations are referred to as longitudinal waves.

When $n = 0$, the determinant in Eq. (2.18) degenerates to the product of two subderminants, i.e.

$$\begin{vmatrix} \Gamma_{11} & \Gamma_{12} & \Gamma_{13} & \Gamma_{14} & 0 & 0 \\ \Gamma_{21} & \Gamma_{22} & \Gamma_{23} & \Gamma_{24} & 0 & 0 \\ 0 & 0 & \Gamma_{33} & \Gamma_{34} & \Gamma_{35} & \Gamma_{36} \\ 0 & 0 & \Gamma_{43} & \Gamma_{44} & \Gamma_{45} & \Gamma_{46} \\ \Gamma_{51} & \Gamma_{52} & \Gamma_{53} & \Gamma_{54} & 0 & 0 \\ \Gamma_{61} & \Gamma_{62} & \Gamma_{63} & \Gamma_{64} & 0 & 0 \end{vmatrix} \tag{2.24}$$

$$= \begin{vmatrix} \Gamma_{11} & \Gamma_{12} & \Gamma_{13} & \Gamma_{14} \\ \Gamma_{21} & \Gamma_{22} & \Gamma_{23} & \Gamma_{24} \\ \Gamma_{51} & \Gamma_{52} & \Gamma_{53} & \Gamma_{54} \\ \Gamma_{61} & \Gamma_{62} & \Gamma_{63} & \Gamma_{64} \end{vmatrix} \cdot \begin{vmatrix} \Gamma_{35} & \Gamma_{36} \\ \Gamma_{45} & \Gamma_{46} \end{vmatrix} = \delta_3 \cdot \delta_4 = 0$$

Considering $\delta_3=0$, this is found to represent the longitudinal modes involving only the displacements u_r and u_z, The displacement field $u_\theta = 0$ is automatically satisfied since $\sin(n\theta) = 0$ when n = 0. As in the case of waves in a plate, these modes involve both *dilatational* and *equivoluminal* waves through the potentials f and g_1. A special class of solutions corresponding to *equivoluminal* Lamé-type modes is found to exist for the special case of $\beta^2 = \gamma^2 > 0$ [68].

The *torsional* modes come from

$$\delta_4 = 0$$

$$A = B = C = D = 0 \quad \rightarrow \quad f = g_1 = 0. \tag{2.25}$$

In this case, only u_θ appears, which is not obvious from Eq. (2.7) where if n = 0 the torsional term vanishes. However, this would not be the case if the alternate solution involving the interchanged $\sin(n\theta)$ and $\cos(n\theta)$ were used. The dispersion equation can be simplified to

$$J_2(\beta a)\cdot Y_2(\beta b) - J_2(\beta b)\cdot Y_2(\beta a) = 0 \tag{2.26}$$

In analogy to the case of cylindrical rod, the lowest mode, corresponding to

$$\beta^2 = \omega^2 / V_S^2 - \gamma^2 = 0 \tag{2.27}$$

is not adequately described by general expression for the displacements. But the field

$$u_\theta = B\cdot r\cdot e^{j(\gamma z+\omega t)} \tag{2.28}$$

satisfies the wave equation and the boundary condition if the condition (2.27) holds. All the physical meanings of this mode are the same as that of a rod.

In general, three classes of modes are recognized, the first two of which have their equivalent in the flat plate. These are

1. Longitudinal axially symmetric modes

   L_{0m} (m = 1,2,3...)

2. Torsional axially symmetric modes

   T_{0m}(m = 0,1,2,3...)

3. Non-axially symmetric modes

   F_{nm} (n = 1,2,3..., m=1,2,3...)

In these modes the integer m refers to the modes of vibration within the wall of the tube, while n refers to the modes of flexing of the tube as a whole. In the case of non-axially symmetric modes F_{nm}, all three particle motions are coupled to one another.

It could be difficult to visualize these modes, but it may be helpful to say that in the limit (as the radius of the tube $r \to \infty$, or the relative wall thickness $h/r \to 0$), the class L_{0m} corresponds to all Lamb waves in a flat plate while the mode T_{00} corresponds to the SH_0 waves in the plate. Fig. 2.2 shows schematically the particle motion in the two lowest axially symmetric modes L_{01} and L_{02} in a longitudinal section of the tube. It can be seen that in both cases the motions are symmetric with respect to the axis, while L_{01} mode is *antisymmetric* and L_{02} mode is *symmetric* with respect to the center of the inner and outer shell surfaces. These two modes asymptotically correspond to the two lowest antisymmetric and symmetric plate modes A_0 and S_0, respectively, as $h/a \to 0$. One will

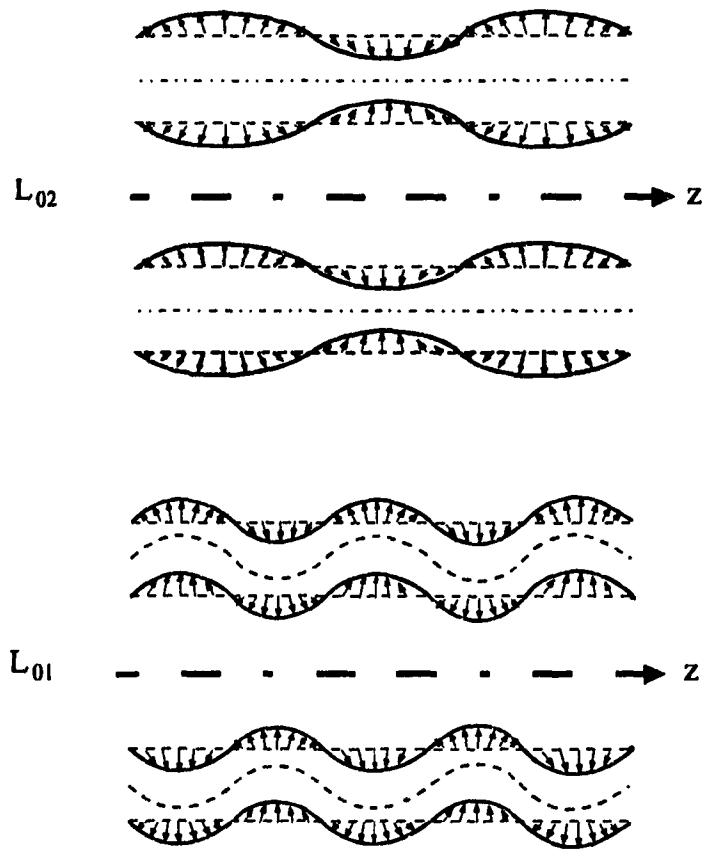

Figure 2.2 Schematic illustration of the particle motion in the two lowest axially symmetric tube modes (longitudinal section of tube).

note that as the inner radius $a \rightarrow 0$, i.e. the tube reduces to a solid cylinder, the L_{01} mode is identical to the lowest axisymmetric mode in a solid rod.

2.1.1 Traveling circumferential waves

The circumferential waves described in Eqs. (2.22) and (2.23) are stationary rather than traveling waves. Along the angular direction, the displacements were described in terms of $\cos(n\theta)$ or $\sin(n\theta)$, where n is an integer.

Viktorov and Zubova firstly discussed the radial-angular plane circumferential waves propagating in cylindrical shells [77], using a two-dimensional theory. They did not discuss the longitudinal-shear modes, i.e. waves with polarization in the axial direction, which correspond to the *SH* modes in the plate case and are also of our interest in sensing application. In their discussion they have presumed the Lamb-like circumferential modes, i.e. waves with polarization in the radial-angular plane, exist without showing that these modes can be *decoupled* from the vibration in the axial direction. They made a quantitative evaluation of the effect of curvature of the thin-walled shell on the normal mode characteristics and obtained asymptotic solutions for the two lowest Lamb-like modes, which correspond to the S_0 and A_0 modes in the thin plate. This corresponds to the case in the three-dimensional theory described above with $\gamma = 0$, $\delta_1 = 0$, and $n >> 1$, i.e., there are many wavelength around the circumference of the shell, and no wave nodes in the thickness direction. By extending our discussions in the three-dimensional theory and properly choosing the potentials, we can easily show that traveling Lamb-like and traveling *SH*-like circumferential modes *can be separated* from each other.

In [68], an *angular wave number* $p = (2\pi / \lambda_r)\, r$ was introduced to describe the traveling circumferential waves, where p is a constant whereas λ_r, and so the phase velocity, is a function of r, as shown in Fig. 2.3. For convenience in our treatment and a better physical understanding of the angular wave number, we further define (see Fig. 2.3)

$$\bar{p} = (2\pi / \lambda_r) \cdot r = 2\pi / \Theta = \omega / \Omega, \tag{2.29}$$

where the parameters Ω and Θ, can be named *angular phase velocity* and *angular wavelength* of the circumferential wave propagation, respectively, as the counterparts of the phase velocity and wavelength of the plate waves in a plate. Here $\bar{p}$, Ω and Θ are all independent of the coordinate r. In order to avoid the artificial limitation on the problem

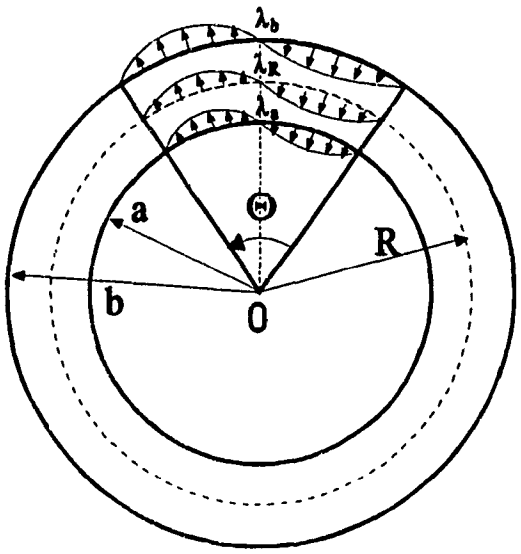

Figure 2.3 Illustration of a circumferential wave with an "angular wave length" of $\Theta = \lambda_r / r$, where $a \le r \le b$.

by integral values of $\bar{p}$, we consider the solution in the infinite angular interval $-\infty < \theta < +\infty$. In this way, different values of the solution in the intervals $m < \theta / 2\pi < m+1$ for various values of the integer m are naturally interpreted as a field consisting of a sequence of *generalized plate waves* [*95*] traversing the cylinder circumference.

We now write the potentials in the form

$$\begin{aligned} \varphi &= f(r)\cdot\cos(\bar{p}\theta + \gamma z + \omega t); \\ \psi_r &= g_r(r)\cdot\sin(\bar{p}\theta + \gamma z + \omega t); \\ \psi_\theta &= g_\theta(r)\cdot\cos(\bar{p}\theta + \gamma z + \omega t); \\ \psi_z &= g_z(r)\cdot\sin(\bar{p}\theta + \gamma z + \omega t). \end{aligned} \tag{2.30}$$

for traveling waves both in the θ and z direction. Replacing Eq. (2.7) with Eq. (2.30), all the equations associated will remain unchanged, except the parameter n is replaced by $\bar{p}$,

the latter being not restricted to be an integer. With $\gamma = 0$, the waves are purely circumferential. From previous discussion, two *independent* classes of modes can be found. The relation between the unknown angular wave number Ω and the parameters α, β and the shell geometry (h, a, b) are defined by $\delta_1 = 0$ for the *radial-angular* modes and by $\delta_2 = 0$ for the *longitudinal-shear* modes, respectively, where the Bessel functions are $\bar{p}$th order rather than nth. The phase velocities of the waves around the outer and inner surfaces of the shell are expressed by $b\Omega$ and $a\Omega$ respectively. When a cylindrical shell with very thin wall is considered, an average phase velocity can be described by $R\Omega$, where R is the average radius of the shell (see Fig. 2.3). By numerically solving the frequency equations $\delta_1 = 0$ and $\delta_2 = 0$, dispersion curves can be obtained for these two types of modes. This is, however, beyond the scope of this thesis.

Practically, asymptotic solutions of the frequency equations are adopted to obtain explicit expressions of the displacement distribution and / or the phase velocity, which are then used to derive explicit formulas for the mass sensitivities of these modes. The few lowest plate modes which are of interest for sensing application, correspond to the axial tube modes of small integers n and m (usually 0 or 1), and to the circumferential modes of very large $\bar{p}$ values (in our tube devices, for example, $\bar{p} \approx 30$), respectively. Furthermore, for the consideration of high sensitivities, we are interested in shells with very thin wall thickness. The condition $h \to 0$ or $a/h \to \infty$ means the arguments αr and βr appearing in the equations are very large. The instability of the asymptotic behaviors of the high order Bessel functions in the limit of large arguments makes it difficult to search the asymptotic solutions, as encountered in the case for the circumferential modes. Efforts in solving this problem by appropriate mathematical transforms and in deriving the related mass sensitivities are being made in parallel with this work in our team by Wang [95], who has recently discussed the asymptotic solutions for the longitudinal-shear circumferential modes and presented the mass sensitivity formulas.

2.2 MASS SENSITIVITIES

In a resonator geometry, the acoustic device is used as the frequency-control element of an oscillator. Perturbations of the oscillating frequency are monitored in response to the changes of the environmental parameters which are considered as the measurands or noise. The mass sensitivity of a resonator configuration is given by [46]

$$S_m^f = \lim_{\Delta m \to 0} \frac{1}{f_0} \frac{\Delta f}{\Delta m} \tag{2.31}$$

where Δm is the mass loaded on a unit surface area of the device, $\Delta f = f - f_0$ and f_0 and f are the unloaded and loaded resonant frequencies, respectively. If the load mass layer is uniformly distributed over the surface and has a density ρ' and thickness h, then

$$\Delta m = \rho' h. \tag{2.32}$$

In an acoustic delay line, a signal of a fixed frequency and amplitude is applied. Changes in the amplitude and/or phase between the input and output transducers due to the perturbations can be determined by measuring the phase velocity and/or attenuation of the propagating acoustic mode. The mass sensitivity in a delay-line configuration is given by [46]

$$S_m^V = \lim_{\Delta m \to 0} \frac{1}{V_0} \frac{\Delta V}{\Delta m} \tag{2.33}$$

where V_0 and V are the unloaded and loaded phase velocities of the delay line, respectively, and $\Delta V = V - V_0$.

According to Rayleigh's hypothesis [4,47], a mechanical resonant system oscillates at a frequency at which the maximum kinetic energy U_k is equal to the maximum potential energy U_p in the same volume. The energy in the form of a potential energy at a particular time will totally convert into a kinetic energy after a quarter cycle. For acoustic gravimetric sensors, if the loaded mass layer is very thin and does not contribute to the elastic property of the resonator, the added layer will not store any potential energy during the vibration cycle. The peak kinetic energy of the perturbed system will therefore remain unchanged for the unperturbed resonator. Based on this hypothesis, the sensitivities S_m^f and S_m^v of the gravimetric sensors comprised of BAW, SAW, plate wave and thin rod wave resonators [4,44,47,56] have been analyzed.

In this section we will estimate the mass sensitivities for two lowest thin-walled tube modes L_{01} and T_{00}, using the approaches developed in [56, 58].

Assuming that a uniform mass layer deposited on an acoustic resonator surface changes the resonant frequency due to the boundary perturbation, we can show that

$$\frac{\Delta\omega}{\omega} = -\frac{\rho'}{4U}\int_S |v_0|^2 ds \tag{2.44}$$

where $\omega = 2\pi f$; v_0 is the total amplitude of the vibration velocity of the particles on the surface of the wave propagating medium; S is the area where mass loading occurs. U is the stored energy of the unperturbed acoustic mode. ρ' and h are the density and the thickness of the loading layer, respectively. The stored energy U in a resonator can be expressed in a kinetic energy form. The total kinetic energy of a mechanical resonator in a volume $\overline{V}$ is given by

$$U = \frac{\rho_s}{2} \int_{\bar{V}} \sum_i |v_i(\mathbf{r})|^2 d\bar{V} \tag{2.35}$$

where ρ_s is the density of the resonator; $v_i(\mathbf{r})$ is the vibration velocity component of the particle loaded at the position **r** and in the ith-direction.

For a tube with an inner radius a and an outer radius b, the kinetic energy U in a volume of $\pi(b^2-a^2)dz$ can be given by

$$U = \left[\frac{\rho_s}{2b} \int_a^b \sum_i |v_i(r)|^2 r dr \right] 2\pi\, b\, dz. \tag{2.36}$$

Thus,

$$S_m^f = -\frac{1}{2\rho\, \Gamma\,(a,b)} \tag{2.37}$$

where, the parameter $\Gamma\,(a,b)$ is the "equivalent depth" [46] of the displacement of a certain acoustic tube mode, and for the case of outer surface sensing

$$\Gamma(a,b) = \Gamma^b(a,b) = \frac{1}{b} \int_a^b |\eta\,(r)|^2 r\, dr \tag{2.38}$$

or, for the case of inner surface sensing

$$\Gamma(a,b) = \Gamma^a(a,b) = \frac{1}{a} \int_a^b |\eta\,(r)|^2 r\, dr \tag{2.39}$$

where

$$|\eta\,(r)|^2 = \sum_i |v_i(r)|^2 / |v_0|^2. \tag{2.40}$$

With the same restrictions and assumptions as for the resonator, the perturbation formula for the phase velocity measurement can be expressed by

$$\frac{\Delta V}{V} = -\frac{\rho'_s h V}{4P_a}|v_0|^2 \tag{2.41}$$

where P_a is the average power flow per unit width and is given by

$$P_a = \frac{1}{2\pi b}\int_0^{2\pi}\int_a^b U_{av} V_g \, r\, dr\, d\phi = \frac{1}{b}\int_a^b U_{av} V_g \, r\, dr \tag{2.42}$$

for a cylindrical shell. V_g is the group velocity of the acoustic propagating mode along the z direction. U_{av} is the average stored energy density,

$$U_{av} = \frac{\rho_s}{2}\sum_i |v_i(\mathbf{r})|^2 \tag{2.43}$$

From Eqs. (2.41), (2.42), (2.43) and (2.44) we have the relation

$$\frac{\Delta V}{V} = \frac{\Delta f}{f}\left(\frac{V}{V_g}\right) \tag{2.44}$$

and thus

$$S_m^V = \frac{V}{V_g} S_m^f. \tag{2.45}$$

For the lowest longitudinal mode L_{01}, which corresponds to the A_0 plate mode, if the tube wall is thin enough the displacement distribution along the radial direction is

considered to be uniform and the contribution of the longitudinal component can be neglected , we have

$$u_r = Ae^{i(\gamma z-\omega t)} \tag{2.46}$$

where γ is the longitudinal propagation constant.

The velocity of vibration is

$$v_r = -\omega A e^{i(\gamma z-\omega t)} \tag{2.47}$$

Thus

$$\Gamma^b(a,b)=\frac{1}{b}\frac{\int_a^b|v_\theta(r)|^2 r dr|}{|v_\theta(b)|^2}=\frac{1}{b}\int_a^b r dr=\frac{(b^2-a^2)}{2b}=h\left(\frac{1+a/b}{2}\right) \tag{2.48}$$

where $h = b - a$ is the wall thickness of the tube.

Similarly,

$$\Gamma^a(a,b)=h\left(\frac{1+b/a}{2}\right) \tag{2.49}$$

Substituting Eqs. (2.48) and (2.49) respectively into Eq. (2.7) gives

$$S_m^f(b)=-\frac{1}{2\rho\,\Gamma^b(a,b)}=-\frac{1}{\rho h}\frac{1}{(1+a/b)} \tag{2.50}$$

and

$$S_m^f(a) = -\frac{1}{2\rho\,\Gamma^a(a,b)} = -\frac{1}{\rho h}\frac{1}{(1+b/a)} \tag{2.51}$$

If the wall is very thin compared to the radius, i.e., $a \approx b$ or $h = b - a << a, b$

$$S_m^f(b) \approx S_m^f(a) \approx -\frac{1}{2\rho h} \tag{2.52}$$

which is the same as the case of A_0 mode of thin plate [45, 56].

If a $\rightarrow$ [illegible], which corresponds to the thin rod case, we have from Eq. (2.50)

$$S_m^f(a) \rightarrow 0 \tag{2.53}$$

and

$$S_m^f(b) \approx -\frac{1}{\rho h} \tag{2.54}$$

which is in agreement with the result for the L_{01} thin rod mode given in [56].

For the lowest torsional mode T_{00}, the displacement has the form (see Eq. (2.28))

$$u_\theta = B r e^{i(\gamma z - \omega t)} \tag{2.55}$$

and the vibration velocity is

$$v_\theta = -\omega B r e^{i(\gamma z - \omega t)} \tag{2.56}$$

Thus

$$\Gamma^b(a,b)=\frac{1}{b}\frac{\int_a^b|v_\theta(r)|^2 r dr|}{|v_\theta(b)|^2}=\frac{1}{b^3}\int_a^b r^3 dr=\frac{(b^4-a^4)}{4b^3}=\frac{h}{4}(1+a/b)(1+a^2/b^2). \tag{2.57}$$

Similarly,

$$\Gamma^a(a,b)=\frac{h}{4}(1+b/a)(1+b^2/a^2) \tag{2.58}$$

Therefore

$$S_m^f(b)=-\frac{2}{\rho h}\frac{1}{(1+a/b)(1+a^2/b^2)} \tag{2.59}$$

and

$$S_m^f(a)=-\frac{2}{\rho h}\frac{1}{(1+b/a)(1+b^2/a^2)}, \tag{2.60}$$

where again, $h = b - a$, is the wall thickness of the tube.

For a $\approx$ b, or $h = b - a \ll a, b$

$$S_m^f(b)\approx S_m^f(a)\approx-\frac{1}{2\rho h} \tag{2.61}$$

which gives the same sensitivity as in the case of SH_0 mode of a thin plate [47, 56].

If $a \rightarrow 0$, i.e. the tube becomes a rod where only the outer surface is used

$$S_m^f(b) \approx -\frac{2}{\rho b} \tag{2.62}$$

which is in agreement with the result for the sensitivity of T_{00} thin rod mode given in [56] where the rod has a radius of a.

We can see that in both case, the mass sensitivities are identical to those of the corresponding thin plate modes, as $h/a \to 0$.

For some modes of higher orders, where explicit expressions may not be available for the derivation of the sensitivity formulas, numerical computations are required. When the effect of the elasticity and inertial of the loaded layer can not be neglected, a two-layer composite should be considered in the analysis of the sensitivities, which have been recently discussed by *Wang et al.* [53, 54] for the planar structures.

In order to demonstrate the use of thin-walled tube wave devices as excellent mass loading sensors, we list in Table 2.1 the mass sensitivities involving BAW, plate and thin rod acoustic wave devices, which were derived using the perturbation approach and collected from the literatures.

Table 2.1 Mass sensitivities for different acoustic gravimetric sensors, where λ is the wavelength, ρ is the density of the devices, d is the thickness for a bulk or plate sensor, a is the radius of the rod, $h = b - a$ is the wall thickness of the tube, and b and a are the outer and inner radii, respectively.

Geometries	Acoustic modes	S_m^f	References
Bulk	$n = 1$ $(d = \lambda/2)$	$1/\rho d$ or $-2/\rho\lambda$	[4, 56]
Plate	A_0	$-1/2\rho d$	[45, 56]
	SH_0	$-1/2\rho d$	[47, 56]
Rod	F_{11}	$-1/\rho a$	[56]
	T_{00}	$-2/\rho a$	[56]
	L_{01}	$-1/\rho a$	[56]
Tube	T_{00}	$-2/\rho h(1+a/b)(1+a^2/b^2)$	This work
	L_{01}	$-1/\rho h(1+a/b)$	This work

CHAPTER 3: DEVICE FABRICATION

3.1. FABRICATION OF THIN-WALLED TUBES

As theoretically indicated in Chapter 2.2, thin-walled tubes are desirable for making the sensing devices with high sensitivity. Tubes with different wall thickness are also necessary for investigation of the dispersive behavior and characterization of the mass sensitivities. Metallic tubes were chosen as samples in our experiments because of their high mechanical strength and relatively high acoustical impedance. Since tubes with desired wall thickness to diameter ratios were not commercially available, and the few available ones were not economic in our case, we fabricated several thin-walled tubes by chemically etching the thick wall ones. Commercially available copper, brass, aluminum and stainless steel tubes with wall thickness of more than 0.25 mm and different diameters were used as the starting samples. These tubes had relatively uniform wall thickness and smooth outer and inner surfaces.

The etchants used for tube samples of different materials and the etching rates are listed in Table 3.1.

To obtain uniformly etched tubes, a set-up was used as illustrated in Fig. 3.1. Before the etching, the bottom of the tube was sealed with wax, as the inner surface of a tube with relatively small inner diameter (3 - 6 mm) can hardly be etched uniformly and is not easy to be polished. The tube sample was held vertically by a holder and immersed into the chemical solution. Driven by a small motor, the tube was rotated about its axis, while the chemical solution was stirred by a spinning magnet. In this way the chemical solution could be kept uniform and the etched particles attached on the tube surface could be

Table 3.1 Recipes for etching samples of different materials.

Sample materials	Chemicals	Etching rates
Copper / Brass	$FeCl_3$ (8 %) + H_2O (92 %)	5 - 10 μm / min.
Aluminum	H_2PO_4 (75 %) + HNO_3 (10 %) + H_2O (15 %)	0.5 -1 μm / min.
Stainless steel	HNO_3 (30 %) + HCl (60 %) +H_2O (10 %)	3 - 8 μm / min.

removed consistently by the stirred liquid. In order to be able to handle easily the thin-walled tubes in later treatment and measurement without damaging them, one or both ends of the tube was not etched, being covered by a protection layer. The etched tubes were polished to reduce the roughness caused during etching. A cylinder whose outer diameter fitted well the inner diameter of the etched thin-walled tube was used as a supporter during the polishing.

With the procedure described, tubes with relatively uniform wall thickness down to about 30 μm and smooth outer and inner surfaces were obtained.

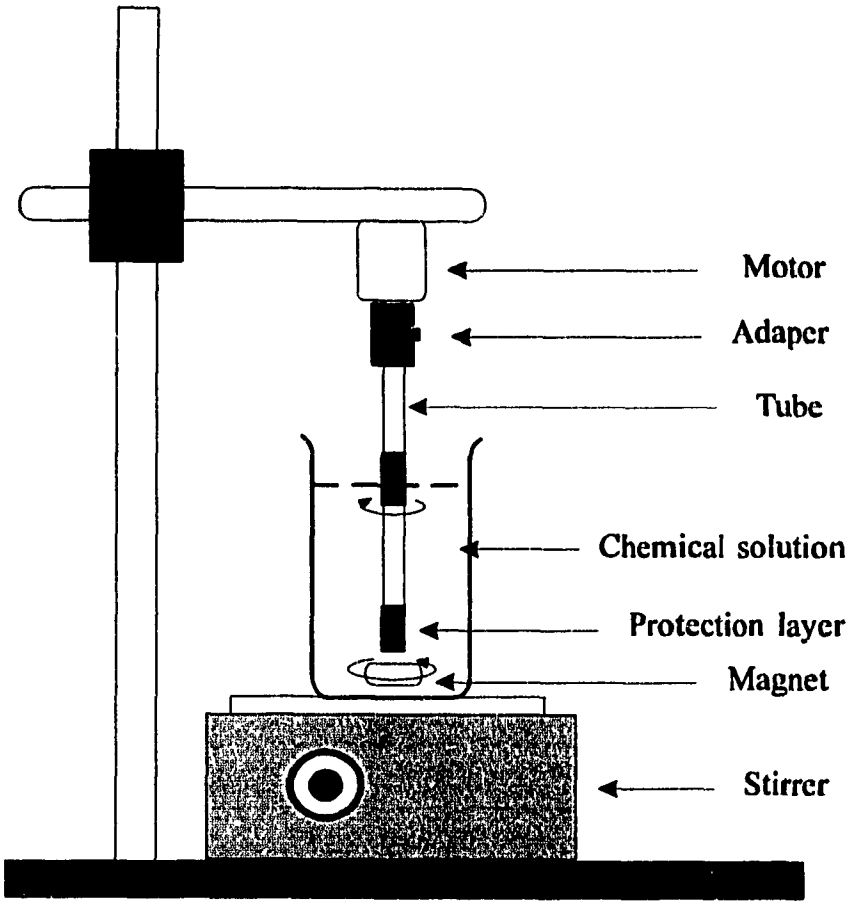

Fig. 3.1 Set-up for tube etching.

3.2 PZT FILM COATING

3.2.1 Sol-Gel process

The sol-gel process is basically a chemical route to the preparation of high purity ceramic and glass materials [91]. In the making of films, a colloidal solution containing the required species is prepared and is then applied to a substrate to form a liquid layer. In order to obtain a continuous film, the liquid layer should be polymerized or gelled to form a solid gel layer. The solid gel layer is then dried and fired to displace unwanted components to form an amorphous inorganic film. In some cases a high-temperature anneal, e.g. for PZT, may be required to develop the desired structure in the final film. The transition from a colloidal solution to a solid gel has led to the expression "sol-gel processing".

The basic principle of preparation of the solution is to dissolve suitable precursors containing the elements of the desired thin film in a proper solvent. If necessary, specific precursors should be synthesized. The solution formed must contain one or more compounds that can be polymerized to form an inorganic network, so that the solution can be gelled after application to substrates. The gelation of the solution is necessary for preparation of thick films.

In the sol-gel processing of thin films, the solution of precursors can be applied to a substrate by dipping, spinning, painting or spraying, etc. The thickness and uniformity of the liquid layer formed on the substrate is determined by the technique of application and the viscosity and surface tension of the solution. The thickness of the final film is determined by the thickness of liquid layer and the metal content of the solution. In device fabrication, especially in industrial processing, thickness control is crucial. To achieve high

uniformity and reproducibility in the thickness of thin films, the solution prepared should be stable under ambient conditions and have appropriate viscosity and surface tension.

The gelation of the liquid layer is caused by the formation of an internal inorganic network due to the hydrolysis and condensation of metal complexes. Gelation can also be produced by rapid evaporation of the solvent or by heating, as occurs during preparation of the films. After gelation, the layer formed on the substrate consists of two phases, the network solid phase and connected pores filled with liquid phase. The unwanted compounds in the gel layer are displaced by drying and firing. The drying of the gel layer displaces the liquid phase, changing the wet gel layer of two phases into porous xerogel layer. The firing of the xerogel layer in air at about 350 °C pyrolizes and oxidizes the organic components left in the layer and converts the xerogel layer to an inorganic film. On heating to higher temperatures, the porous amorphous inorganic film will either densify to become a pore-free glass or crystallize to become a ceramic film.

A. Preparation of solution for sol-gel PZT films

A novel sol-gel process for preparation of PZT films has been recently developed by Yi *et al* and a typical recipe of the stock solution for PZT films was given in [85, 92], where Lead acetate, $Pb(OOCCH_3)_2*3H_2O$, zirconium propoxide, $Zr(OC_3H_7)_4$ (70% wt.% solution in normal propanol) and titanium isopropoxide, $Ti[OCH(CH_3)_2]_4$, were used as precursors. They are commercially available with high purity and at reasonable prices.

Lead acetate was selected as the source of lead because of its high solubility and stability in water. The solutions of zirconium propoxide in normal propanol and titanium isopropoxide were selected as the source of zirconium and titanium respectively. They can be modified with acetic acid to form highly soluble zirconium propoxide acetate and

titanium isopropoxide acetate, which are chemically compatible with each other and also with lead acetate. Furthermore, they can be polymerized in aqueous solutions.

A suitable solution for sol-gel films should be stable under ambient conditions and be able to polymerize after coating on the substrate to form a gel film without disturbance of its homogeneity. The metal content needs be high enough to build up the desired thickness of the final film. The solution is required to exhibit appropriate viscosity and tension and can be applied on the substrate uniformly. In the gel film the unwanted components should be removed easily by evaporation, pyrolysis and oxidation. The gel films formed must not crack or peel from substrates during processing. With these considerations, a special solution for sol-gel PZT films has been developed [85, 92].

Lead acetate was dissolved in heated acetic acid in a proportion of one mole of lead acetate to five moles of acetic acid. The solution was then heated to 100 °C for 10 minutes to remove water since water may cause non uniform gelation of titanium isopropoxide and zirconium propoxide. The dehydrated solution was then cooled to room temperature. The required quantity of titanium isopropoxide and the solution of zirconium propoxide in normal propanol were mixed to form a solution with a specific molar ratio of titanium to zirconium. The resulted solution exhibited higher viscosity than titanium isopropoxide and the solution of zirconium propoxide in normal propanol before mixing. Since PZT ceramics have the highest dielectric constant and show the strongest piezoelectric properties near the morphotropic composition, typical solutions prepared have the morphotropic composition with a Ti/Zr molar ratio of 46.5/53.5 [92] .

The solution containing Pb and the solution containing Ti and Zr were mixed in a proportion of one mole of Pb to one mole of Ti and Zr. When mixing these two solutions, heat was evolved, resulting in a clear solution. This solution is not a stable system in

equilibrium and if left at room temperature, crystalline particles and condensed solids would form. Therefore, before the solution was cooled, distilled water was added in a proportion of twenty to forty moles of distilled water to one mole of lead. The quantity of the distilled water is also determined by the desired viscosity of the final solution. The more distilled water that is added, the lower is the viscosity of the final solution, and thinner films may be prepared. After adding distilled water, the solution became a relatively stable system in which precipitates and condensed solids would not form. However, over a period of about three days, the viscosity of such a solution would increase and a transparent gel could form.

In order to obtain a stable solution with constant viscosity, lactic acid was added into the solution in a proportion of one mole of lactic acid to one mole of lead. The more lactic acid that is added, the lower is the viscosity of the final solution. After adding in lactic acid, the solution was stable and did not gel for several months.

At this stage, the solution can be applied onto a substrate to form a liquid film. However, the formed solid films would not show good mechanical properties and have a strong tendency to crack and to peel from the substrate upon drying. In order to improve the mechanical properties of the gel film, ethylene glycol and/or glycerol were added into the solution in a proportion of one mole of ethylene glycol and/or glycerol to one mole lead. Also, the quantities of ethylene glycol and glycerol to be added are determined by the thickness of the gel film required. The thicker the gel film is desired, the more ethylene glycol and/or glycerol should be added. The sequence of addition of the chemicals should not be changed since reactions of titanium isopropoxide and zirconium propoxide with ethylene glycol, glycerol and water can lead to irreversible gelation and precipitation.

The solution was then filtered using a membrane filter with a pore size of 0.22 μm. The final solution was stored in a clean sealed container. Some solvent could be removed by heating the open bottle in air or in an oven to increase its viscosity. However, if the solution is heated to about 100 °C in air or in vacuum, it will gel. The solution should be aged for at least three days before preparation of the films. The aged solution exhibited a constant viscosity and gel films prepared with the aged solution showed a lower tendency to crack and to peel from the substrates.

A single fired layer of 0.3 ~ 0.5 μm in thickness can be obtained from the typical solution by spin or dip coating. Thinner films could be prepared by adding some combination of water and propanol to dilute the solution. The addition of propanol lowers the surface tension of the solution and can improve the wetability of the solution for substrates of different materials. Thick films may be built up by a multilayer coating process.

B. Substrate surface treatment

Fabrication of films free of defects and cracks requires a dust-free environment and special attention must be paid to the film adhesion. A large internal stress is caused by the volume change between a wet coating and a fired film. Mismatch of thermal expansion between the film and substrate can also result in cracking. However, if the adhesion between the film and substrate is strong enough so that the internal stress is dispersed uniformly in the film and stress concentrations due to spots of poor adhesion do not exit, the films will not crack during firing and the internal stress can be partially relaxed upon annealing.

The substrate surfaces to be coated were polished. Substrates were boiled in water and detergent before final rinse in distilled water. Organic contaminants were removed by ultrasound and by vapor degreasing in methanol. The substrates were then rinsed in boiling filtered distilled water and blown dry with filtered nitrogen. Heating up the substrates to about 400 ^{0}C further removed the organic substances that may remain.

In order to increase the adhesion between the PZT film and the substrate surface, a thin intermediate layer can be introduced on the surface prior to the deposition of the PZT layer. Layers of Al_2O_3, MgO, ZrO_2 and TiO_2 were considered for this purpose, Al_2O_3 being the best choice [85]. For some metallic substrates, such as Aluminum and stainless steel, a thin condensed oxidation layer can be formed by heating up the substrates in air and no additional deposition is required [93].

C. Application of films on substrates

Dip-coating and spin-coating are commonly used techniques in sol-gel process. Others are painting and spraying. In a dipping process the sol film flows down the substrate after wetting the surface. Because it wets the surface, it partly adheres. When the film reacts with the moisture in the atmosphere it undergoes hydrolysis and condensation. For a given solution, the thickness d of the film is proportional to the drawing speed V to a power of 2/3 [91]

$$d \propto V^{\frac{2}{3}}$$

One distinct advantage of this technique is homogeneous and uniform films can be obtained for substrates with large areas or complex shapes [e.g. 88,89]. Another feature is that it is possible to coat all over, inside and outside the component, where necessary.

Spin coating is a technology that has been well developed by the micro-electronics industry for the application of thin photoresist layers onto the semi-conductor wafers. It has been applied to sol-gel coating for thin planar substrates, e.g. in developing BAW and SAW devices with PZT films [86]. This method consists of dropping a quantity of sol onto the substrate which is spinning at a high speed, e.g. 3000 r.p.m. This gives very uniform films. Further advantages are that it is economical in usage of solution and only one surface needs to be coated. Disadvantages are edge effects on non-axisymmetric substrates and the mechanical problems associated with spinning large substrates. The thickness control is a little easier than dip coating and is governed by the spin speed and the viscosity of the solution. While dip coating was our choice for tubes, spin coating was also performed to coat PZT films on planar substrates as comparison.

D. Firing of precursor films

The firing process which changes the organic precursor film into an inorganic ceramic film by the pyrolysis of organometallic compounds is a key step in the film preparation. The firing schedule affects film cracking, crystal structure, grain size and surface roughness.

During the firing, the solvents evaporate with a consequent large change in volume and the generation of internal stress. This occurs in the range from room temperature to 250 °C. Then the lead acetate dehydrates, melts and decomposes. The dried film becomes "wet" again and the organic compounds begin to decompose. The internal stress is relaxed and the volume change of the film continues. the organic film then changes to a fine mixture of oxides of Pb, Ti , Zr and free C. At higher temperature, the free carbon oxidizes and the mixture of oxides transforms to a transparent amorphous PZT film.

Firing the film at a relatively high firing temperature and a rapid increase of temperature reduces the tendency of cracking. The limit of firing temperature for thick film was between 350 and 500 °C [92].

E. Annealing

As-fired PZT films are basically amorphous and annealing is required for the crystallization to form the perovskite structure [85] . This process was done using a temperature-time profile in which the annealing temperature was progressively raised, then maintained at a constant temperature (500 - 600 °C) for a period up to 6 hours, depending on substrate materials, and finally reduced in successive 2-hour interval to room temperature. More recently, rapid annealing of PZT films at 700 °C for 3 seconds was also reported [96].

F. Poling

The sintered PZT films do not show piezoelectricity. As a class of ferroelectric materials the PZT ceramics exhibit dipole moments. Above a certain temperature, known as Curie point, the dipoles have random orientations. Below the Curie temperature, an unpoled ferroelectric material like PZT contains small domains, in which the dipoles are spontaneously aligned. The directions of the aligned dipoles in different domains, however, are randomly oriented with one another, and therefore macroscopically the material is non-piezoelectric. These domains can be aligned by applying a strong DC electric field (~ 20 kV/cm for PZT) at a temperature near the Curie point, while slowly decreasing the temperature. This process is known as *poling*. The poling process aligns the great majority of individual domains and causes the PZT films piezoelectric.

3.2.2 Coating PZT films on tubes

A special recipe of the stock solution was designed for coating PZT films on metallic tubes by means of dipping, as listed in Table 3.2. The solution prepared was contained in a thin and tall glass bottle suitable for tube dipping.

The tube substrates were cleaned as described in 3.2.1 (B). Before the coating, a substrate was pre-heated at a temperature of about 500 °C to remove possible remaining organic substances and to form an oxidation layer on the metallic substrate surface, which is important for good adhesion.

Table 3.2 A recipe of stock solution for PZT films coating on metallic tubes

Chemicals		Quantities
Lead acetate	$Pb(OOCCH_3)_2*3H_2O$	12.00 g
Acetic acid	CH_3COOH	3.00 g
Zirconium propoxide (70wt. % in 1-propanol)	$Zr(OC_3H_7)_4$	7.92 g
Titanium isopropoxide	$Ti[OCH(CH_3)_2]_4$	4.18 g
Lactic acid	$CH_3CHOHCOOH$	0.5 g
Ethylene glycol	$HOCH_2CH_2OH$	0.7 g
Glycerol	$HOCH_2CHOHCH_2OH$	5.5 g
Distilled water	H_2O	50.0 g

Fig. 3.2 illustrates an automated dipping - firing system. The sample holder can move vertically and horizontally through the translation stages, driven by stepping motors The tube substrate was hung on the sample holder in a manner such that its axis could be kept vertical with its own weight during dipping. The bottom opening of the tube substrate was sealed since only the outer surface was intended to be coated. Some weights were inserted in the tube before sealing. the sample was lowered down and immersed into the solution by a depth of the desired coating length. The sample was then withdrawn up at a speed of ~ 1.5 cm / minute, as programmed, until the whole tube was out of the solution. After drying in the air for about 10 minutes, the sample was moved to a vertically mounted tube-furnace and was then located at the central zone of the furnace. The firing was carried out at a temperature of 475 °C for 6 minutes. The sample was then automatically taken out, staying in the air until cooled down to the room temperature. By repeating the above procedure, multilayer coating was performed and films of up to 20 coats were obtained. The whole procedure was carried out by a programmable control system using a PC computer.

The as-fired films coated on stainless steel substrates were annealed at 600 °C for 2 hours and those on aluminum substrates were treated at 520 °C for 8 hours, respectively.

Following the above procedures, crack-free PZT films of thickness up to 6 μm were successfully coated on stainless steel tubes of diameters 6 mm - 10 mm, with a coating length up to 100 mm. The coating length was limited by the temperature-homogeneous zone of the furnace used. Fig. 3.3 shows a part of a radial cross-section of a PZT coated stainless steel tube with a wall thickness of 0.5 mm and an outer diameter of 9.6 mm. The PZT film thickness is estimated to be about 5 μm.

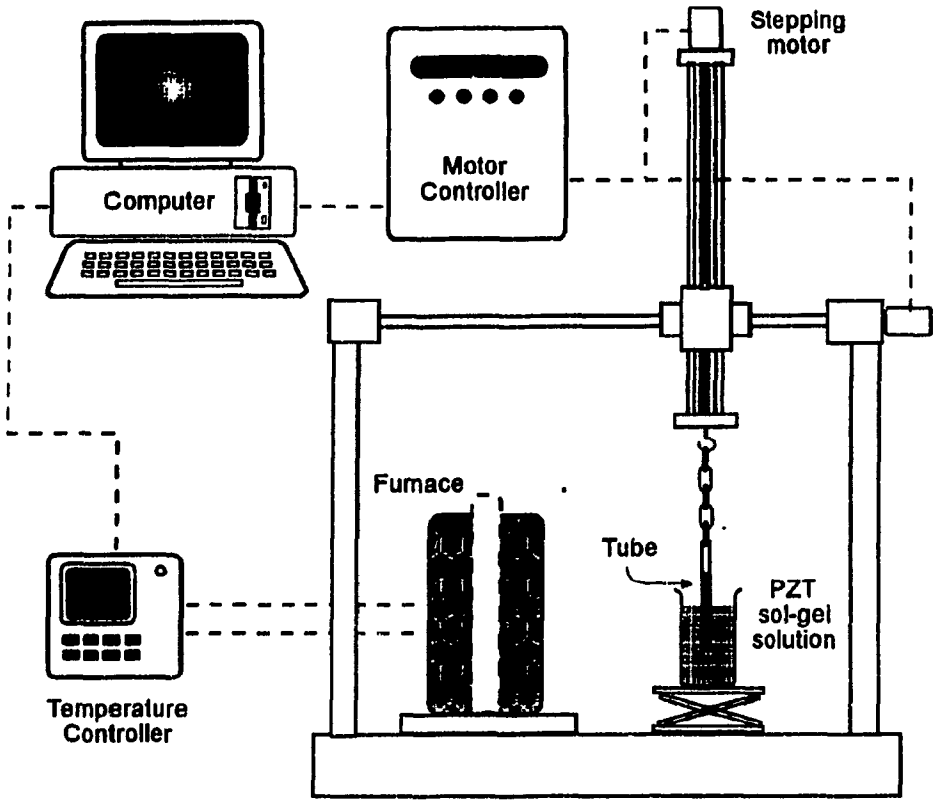

Figure 3.2 An automated system used for dip-coating and firing the PZT film on tubes.

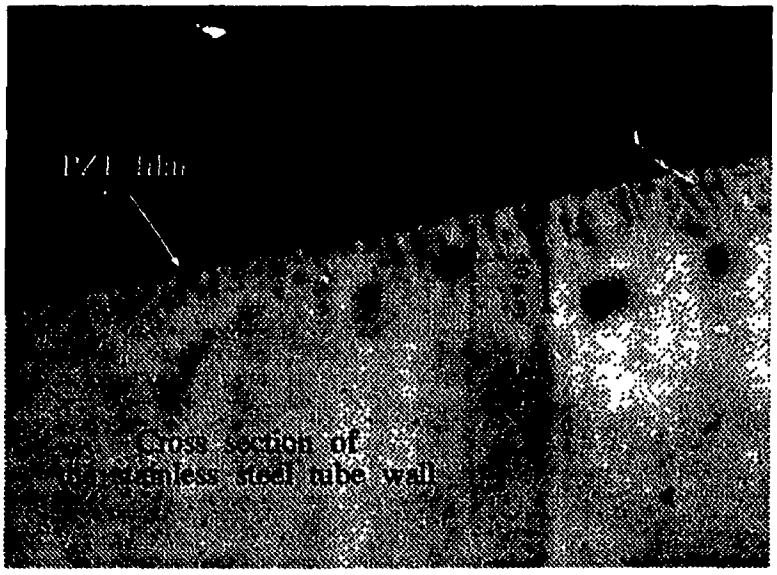

Fig. 3.3 A radial cross-section of a stainless steel tube with a wall thickness of 254 μm, coated with a 5 μm thick PZT film.

Fig. 3.4 (a) presents the X-ray diffraction patterns of the PZT film coated on a stainless steel tube. It is identical to those reported in [92,93] and indicates the film has the perovskite structure.

In the coating of the aluminum tubes, up to about 12 coats (corresponding to about 3.5 μm thick), the PZT films were found still free of cracks after fired at 450 °C. Further coating resulted in micro cracks in the film when fired. After an annealing at 600 °C for 2 hours, the film cracked severely and even peeled off from the aluminum tube. This is due to the relatively high thermal expansion coefficient and low melting point (about 660 °C) of aluminum.

A way to solve this problem could be annealing the film at lower temperature for longer time, since the PZT is able to crystallize at a much lower temperature on aluminum substrates than on others [92, 93]. We then annealed the aluminum tubes coated with up to 10 PZT layers at 520 °C for 8 hours, rather than at 600 °C mentioned above. The final films were found much improved, though not as good as those on the stainless steel substrates and some areas of micro cracks were still observed under the microscope. These films were evaluated by the X-ray diffraction which showed the desired crystalline structure (Fig. 3.4 (b)). Further improvement of the PZT films on aluminum substrates requires a combination of adjustment of the chemical solution and a modified firing and annealing procedure.

The PZT films coated on the tubes were poled by applying a DC voltage cross the film thickness, using the tube itself as one electrode and an aluminum layer (~ 0.2 μm thick) coated on the PZT film surface as another, (the latter being also used to form the IDT's, fabrication procedures of which will be given in the next section). The sample was

kept at 185 °C for two hours with an applied DC voltage of about 3 V per 1 μm of film thickness, and then slowly cooled down to room temperature.

Before going to the next stage of IDT fabrication, a simple way was used to check the piezoelectricity of the films obtained from the poling. An AC signal was applied across the film thickness and at certain frequencies (~ 10 kHz), which may be the acoustic resonant frequency of the tube, a sound of ringing was clearly heard.

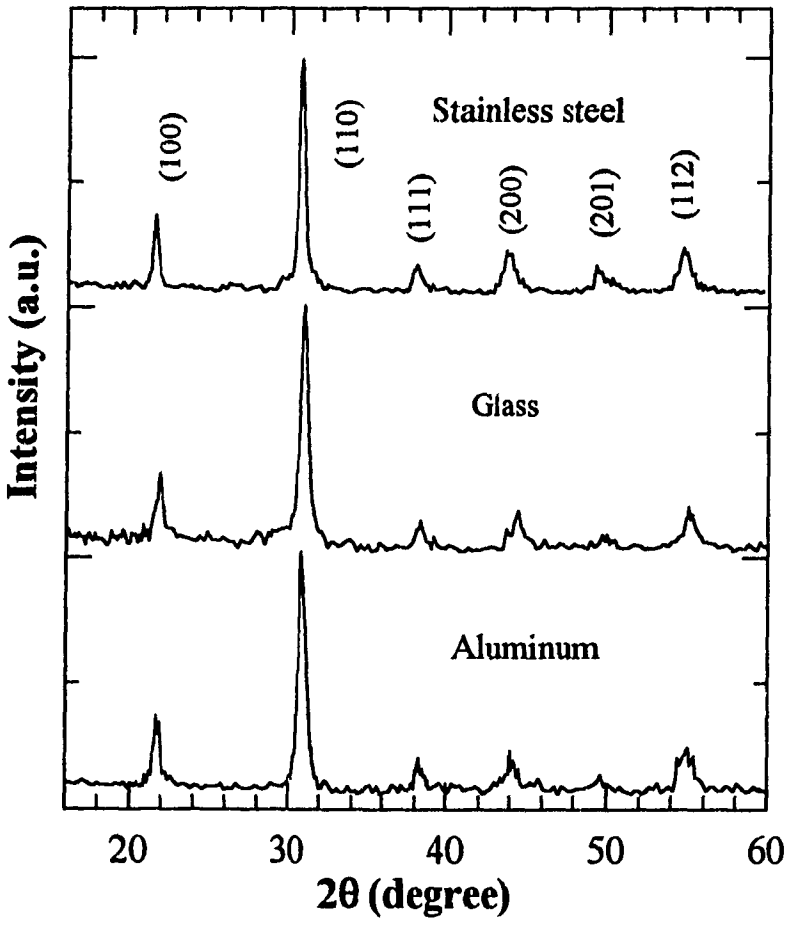

Figure. 3.4 X-ray diffraction patterns of the PZT films coated on a stainless steel tube (top curve), an aluminum-coated glass tube (middle curve) and an aluminum tube (bottom curve).

3.3 INTERDIGITAL TRANSDUCERS ON TUBES

Common photolithographic techniques for fabricating SAW and thin-membrane devices were applied in making the interdigital transducers (IDT) on the tube devices. Some modifications were taken due to the curved tube surfaces.

The classical and still commonly used method in photolithography is aqueous chemical etching. It has numerous versions, but essentially involves the deposition in vacuum of the desired metal film (e.g. 2000 Å aluminum) on a piezoelectric crystal that has been previously polished, carefully cleaned and degreased [e.g. 93]. A photoresist layer is coated on the metal film and then exposed (in general, with UV light). Finally, after appropriate development and baking of the photoresist, the unprotected metal is etched. Fig. 3.5 (a) illustrates this process.

Another method is the *lift-off technique*. In this process the photoresist is deposited directly on the substrate, an "inverted" mask is exposed, unwanted photoresist is removed, and metal is then deposited over the entire surface of the sample. Finally, the photoresist is dissolved with a solvent (in general, acetone). All that remains is the metal lodged between the photoresist tracks, as illustrated in Fig. 3.2 (b). This technique also gives good resolution and is applicable for chemically reactive substrates. Using this method may reduce the risk to damage the PZT film. However, as implied in Fig. 3.2 (b), the lift-off process requires that the side walls of the photoresist be strictly vertical and the particle beam of the metal being deposited be parallel to these side walls, so that there is no continuity between the metal deposited in the gaps and that on the photoresist. Therefore, this technique is limited only for small angle coating on tubes with large curvature radius.

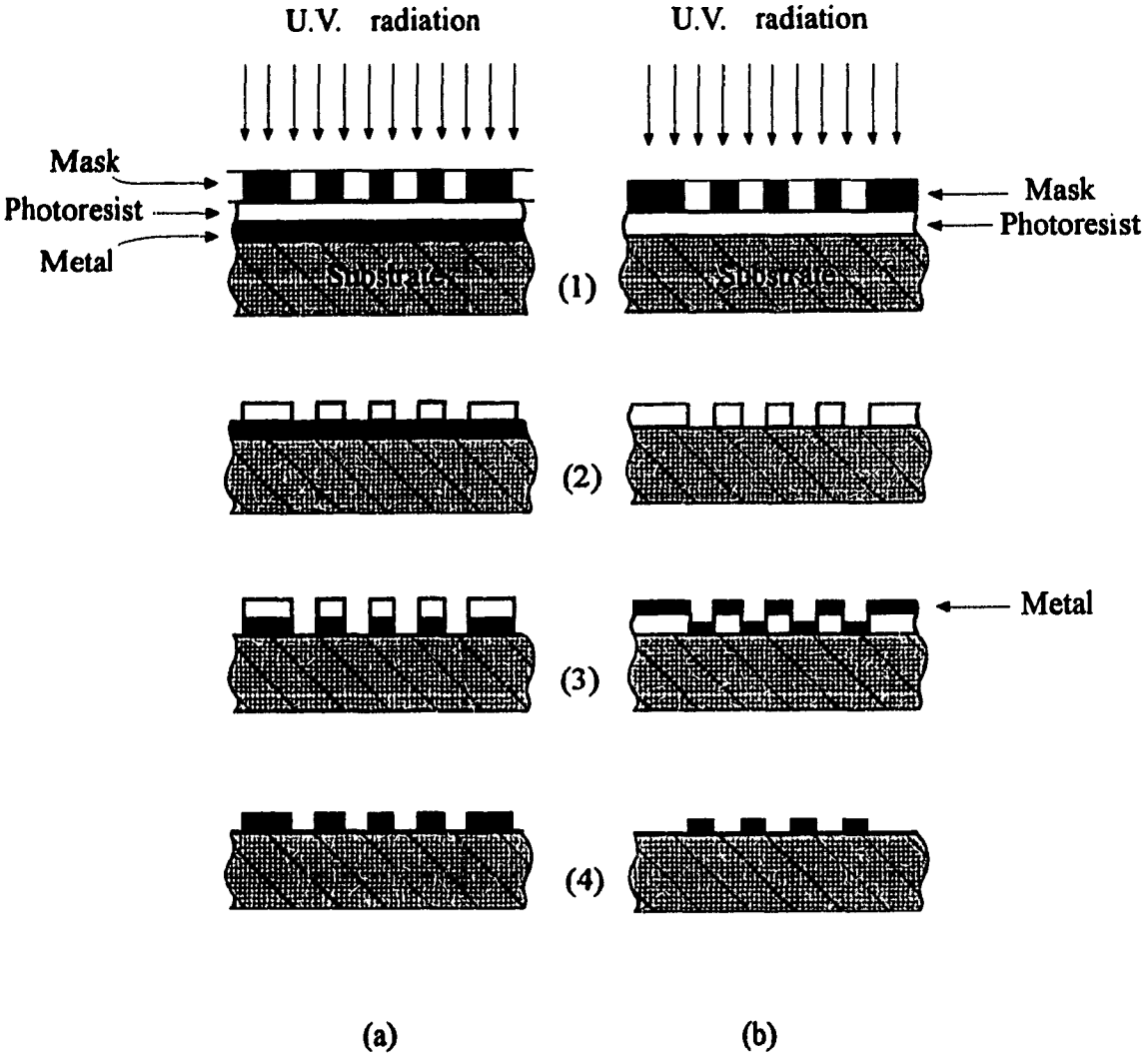

Figure 3.5 (a) Etching technique : (1) deposition of metal, Coating with photoresist, exposure; (2)after development; (3) after chemical etching; (4) After cleaning. **(b)** Lift-off technique: (1) Coating with photoresist, exposure; (2) after development; (3) deposition of metal; (4) after cleaning.

In order to transfer the designed IDT patterns on the curved surface of a tube, masks made of flexible and highly transparent thin films were prepared. The IDT patterns

used were designed as shown in Fig. 36. The IDT had and an aperture of 6.5 mm and 8 finger pairs, with an equal finger width and spacing of 0.25 mm. Along the axial direction, two IDTs were used and the center-to-center distance between the IDTs was 18 mm.

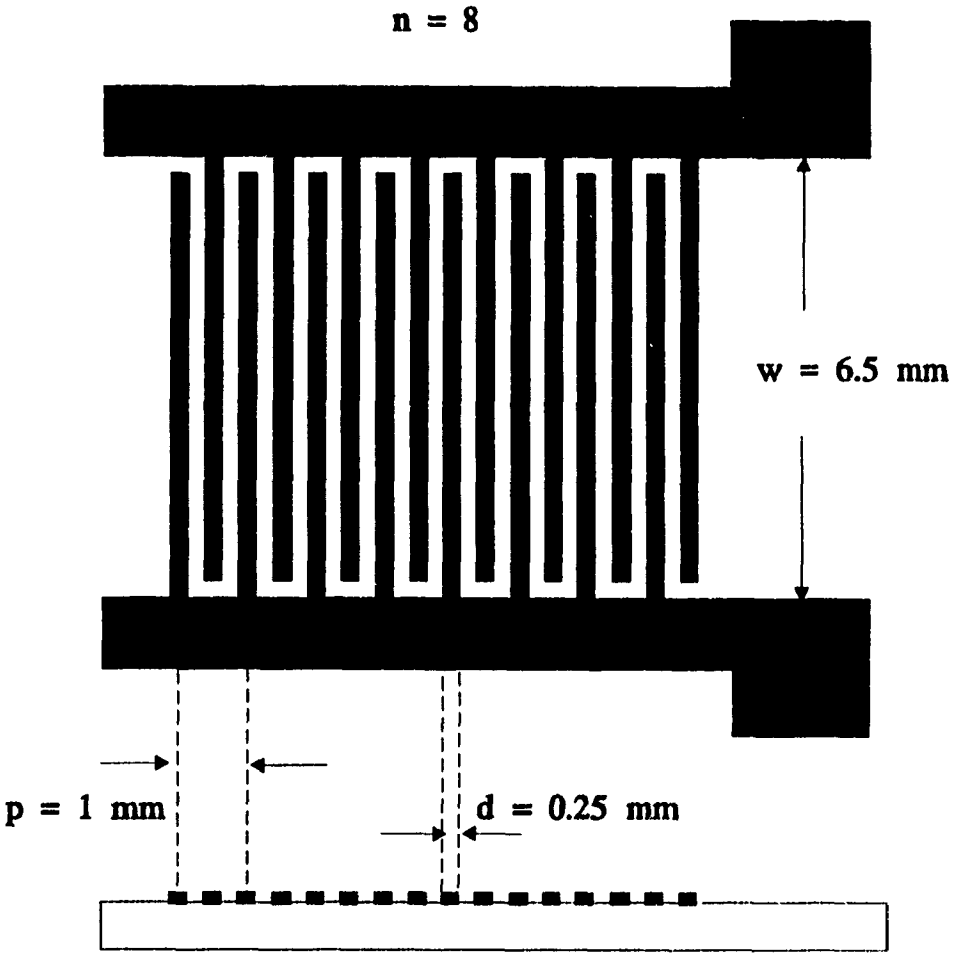

Figure 3.6 Design of the IDT pattern, where n is the number of the finger pairs, p is the distance between a finger pair, and d is the finger width and the spacing.

The etching process was chosen in our fabrication of IDT on tube wave devices. The surface of an annealed PZT film of good quality is smooth enough for our low frequency application where the wave length is much larger than the dimension of the roughness, and ready for photolithographic processing without further polishing. However, cleaning of the film surface is necessary, as the edge effect of the geled PZT films may result in fine particles during the firing, which may slightly pollute the sample surroundings. The cleaning was done with acetone, followed by a rinsing with distilled water and drying with blowing nitrogen.

An aluminum layer of about 1000 - 2000 Å was first deposited on the PZT-coated tube surface by means of vacuum evaporation The tube was mounted in the bell jar with the axis perpendicular to the tungsten wire to maximize the coating angle, as illustrated in Fig. 3.7. In the case where a larger coating angle was required, more than one deposition was performed with the tube rotated by an angle between the depositions. When more uniform electrode thickness is sought, as for devices working at high frequencies whose IDT fingers will be very fine, the tube must be rotated at high speed during the evaporation deposition, with an additional rotating mechanism introduced in the system.

The photoresist coating on the tubes was carried out using the same dipping technique as for the PZT coating. For a given photoresist of certain viscosity, the film thickness is determined by the drawing speed. As mentioned in Section 3.2.1 (C), the lower the lifting speed, the thinner the film obtained. However, reducing the film thickness by slowing down the dipping is not as effective as by increasing the spin speed in a spin-coating and has a lower limit. In order to obtain desired coating thicknesses, the photoresist should be diluted or low viscosity photoresist should be used.

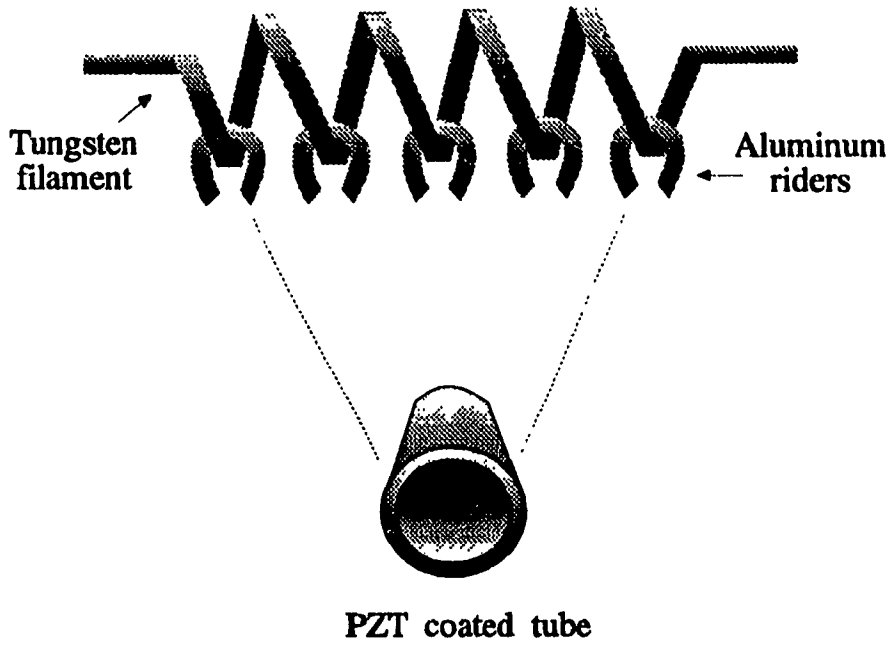

Figure 3.7 Arrangement of tube substrate in metal evaporation

In our experiment, Shipley 1813 Photo Resist was used and diluted with Shipley P-type Thinner by a ratio of 1 part of photoresist to 1.5 part of thinner in volume. With a drawing speed of 1.2 cm / min, a thickness of about 1.5 μm was obtained, which corresponds to that obtained from spin-coating at 3000 r.p.m. for the same type of photoresist without being diluted. The photorisist film coated on the tube was soft-baked in a furnace for 30 minutes at 95 °C, and was then taken out automatically as programmed, with the same system illustrated in Fig. 3.2. The flexible mask film was then placed in close contact with the photoresist layer on the tube, and fixed with a specially prepared clipper. A 150W ordinary floodlight lamp was used as the radiation source, which gave satisfactory resolution for our application in low frequency devices. The sample was exposed for 8 minutes, during which time the tube was rotated to have uniform illumination. The exposed sample was developed for 2 minutes in the Shipley 351 Developer which was diluted with deionized water by a ratio of 1 : 3.5 (developer to

water) in volume, followed by cascaded rinses with deionized water. The tube with the developed photoresist film was then put in a furnace for a hardening bake at 105 °C for 30 minutes. After the hardening bake, a solution of the mixture of 80 ml phosphoric acid, 5 ml nitric acid and 10 ml distilled water was used to etch the aluminum layer in the exposed areas. This gave an etching rate of about 2000 Å / min for aluminum film without harming the PZT layer. The unexposed photoresist was removed with acetone.

Following the above procedure, IDTs were successfully fabricated on PZT-coated stainless steel tubes of different diameters. Fig. 3.8 and Fig. 3.9 show the photographs of the IDTs equipped on thin wall stainless steel tubes with different diameters, along the axial and circumferential directions.

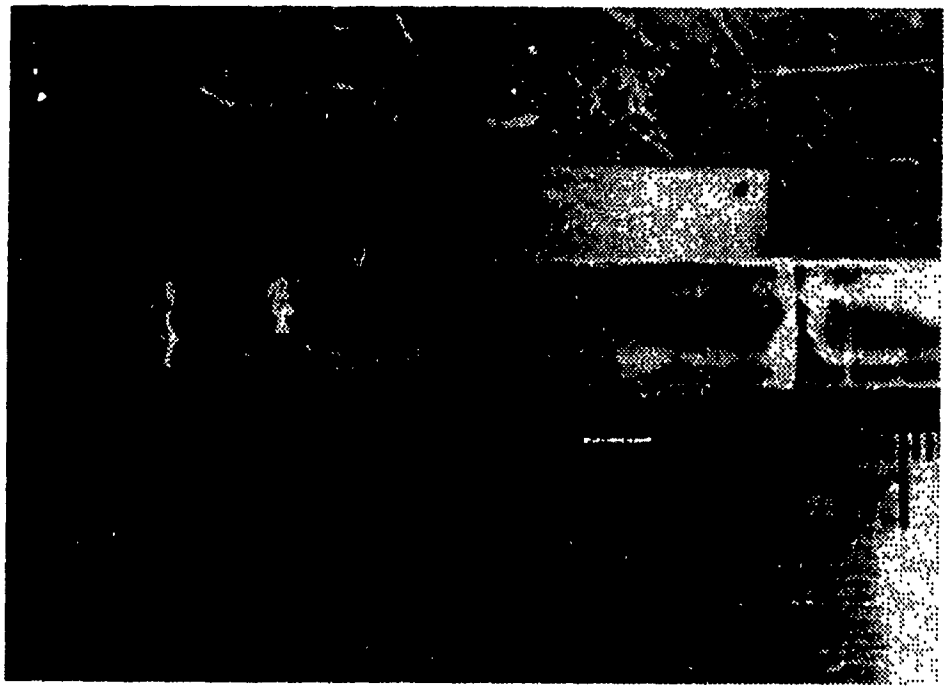

Figure 3.8 Photograph of two IDTs made on a stainless steel tube with an outer diameter of 9.6 mm, along the circumferential direction.

(a)

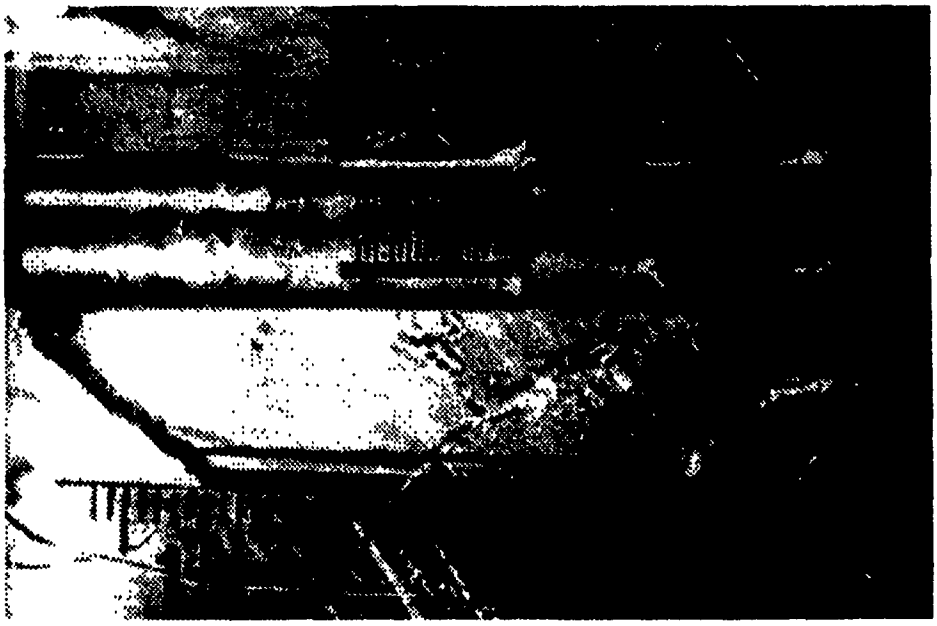

(b)

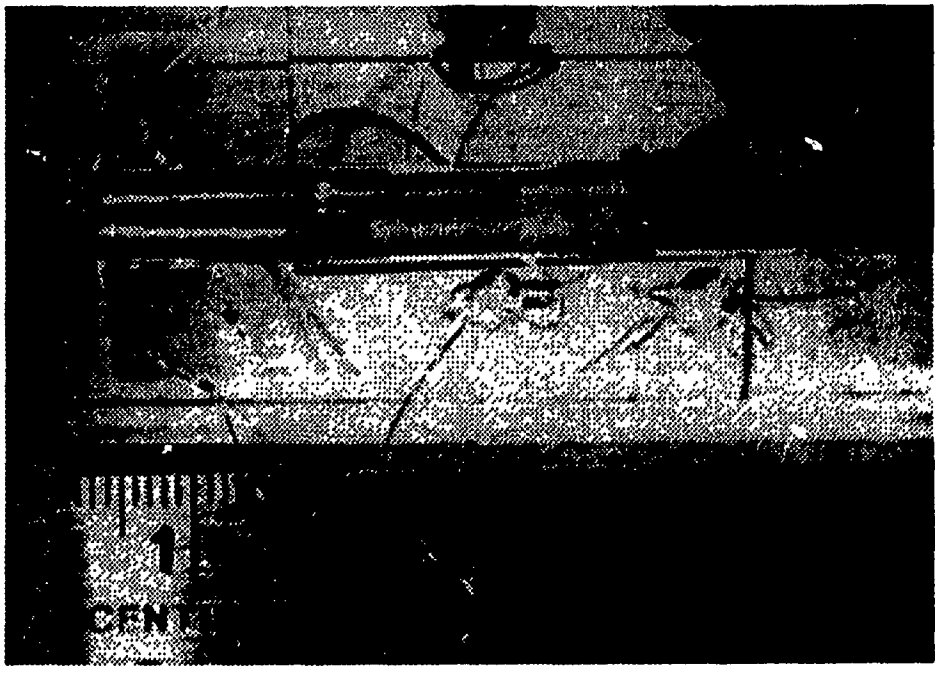

Figure 3.9 Photographs of IDT pairs made on stainless steel tubes with outer diameters of (a) 9.6 mm and (b) 6.0 mm, respectively, along the axial direction.

CHAPTER 4: MEASUREMENT AND EVALUATION OF THE TUBE WAVE DEVICES

The time delay of the waves in the PZT-coated stainless tubes was measured by means of the tone-burst method, using a Ritec Ram-10000 system. In the arrangement as illustrated in Fig. 4.1, along the axial direction of the tube, RF tone bursts were applied to one IDT transducer, and the signals received from another transducer, amplified by the Ritec, were observed on an oscilloscope. Along the circumferential direction, a single IDT served as both the transmitter and receiver. In this case the time delays between the successive "echoes" , i.e. the acoustic signals arriving at the IDT after traveling different cycles along the circumference, were measured. The ultrasonic pulse travels at the group velocity v_g, which can be determined from the delay time t_g between the input and output, by the relation

$$v_g = \frac{l}{t_g} \tag{4.1}$$

where l is the center-to-center distance between the transmitting and receiving IDTs in the axial direction, or the circumference of the outer surface of the tube when a single IDT was used along the circumferential direction. The cross-correlation technique was used to determine the group delay.

In order to observe the frequency response of the IDTs and the dispersive behaviors of the waves excited in the PZT coated thin wall tubes, measurements were performed at different frequencies, ranging from 0.2 MHz to 8.4 MHz. The signals received on the oscilloscope were digitized and the data were acquired to the computer for further processing.

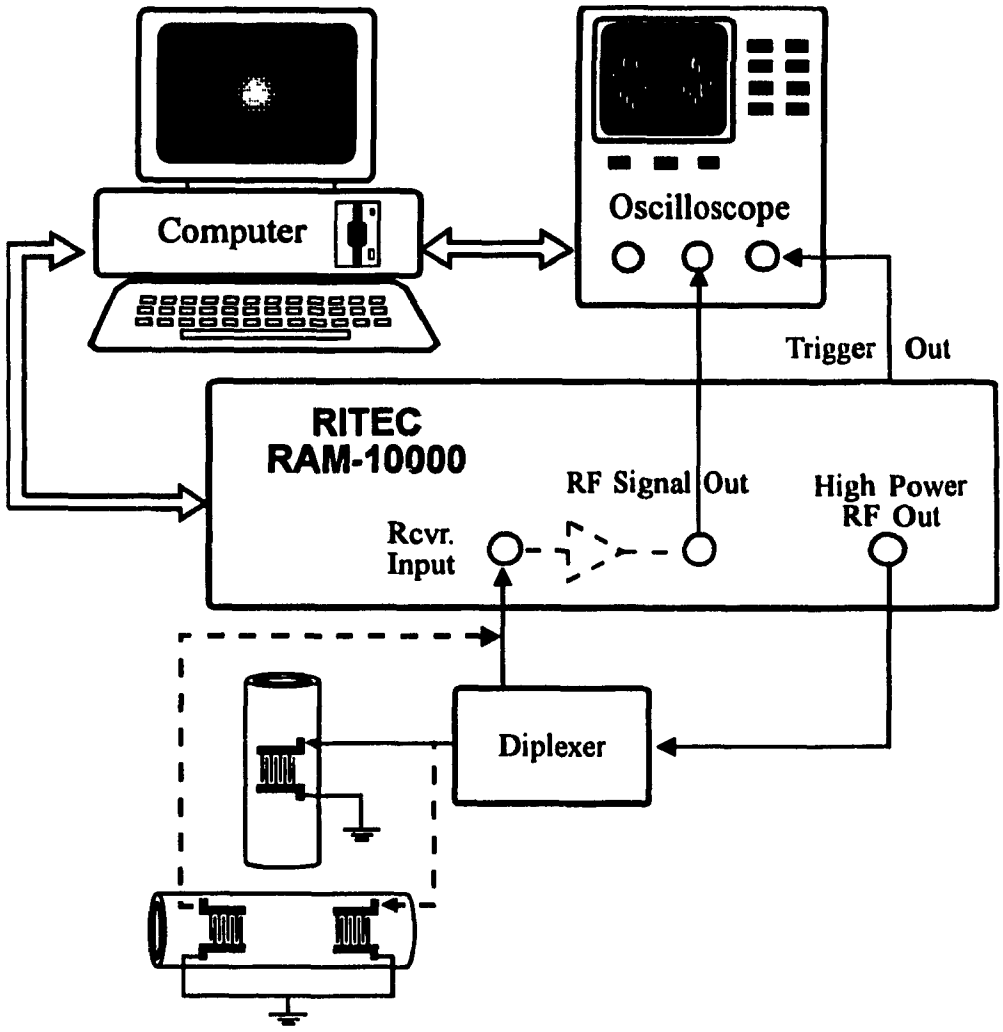

Figure 4.1 Arrangement for time delay measurement of the tube wave devices.

Fig. 4.2 shows the results of the measurement performed with a single IDT on a stainless steel tube with an outer diameter of 9.6 mm and wall thickness of 0.254 mm (sample No. 1) along the circumferential direction at different frequencies. The successive echoes represent the acoustic signals arriving at the IDT after traveling different cycles around the circumference of the tube. Signals of maximum amplitude and best signal to noise ratio were obtained at 2 MHz. It can be seen in Fig. 4.2 that the time delays, and thus the group

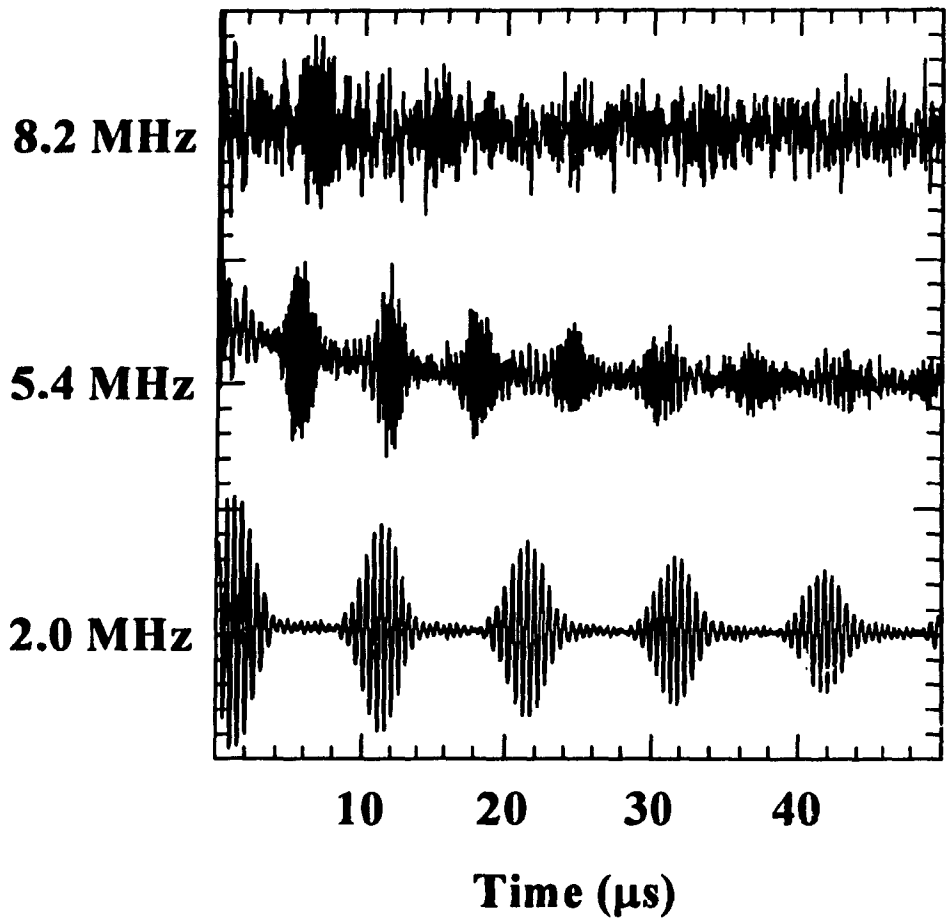

Figure 4.2 Signals of acoustic waves along the circumferential direction of a PZT-coated stainless steel tube with a single IDT.

velocities of the circumferential waves at 2.0, 5.4 and 8.2 MHz are apparently different. The frequency response for the above sample over a range from 0.2 to 8.4 MHz is shown in Fig. 4.3. Peak amplitudes are found at frequencies 2 MHz, 5.4 MHz and 8.2 MHz, respectively, which correspond to the signals measured in the time domain given in Fig. 4.2.

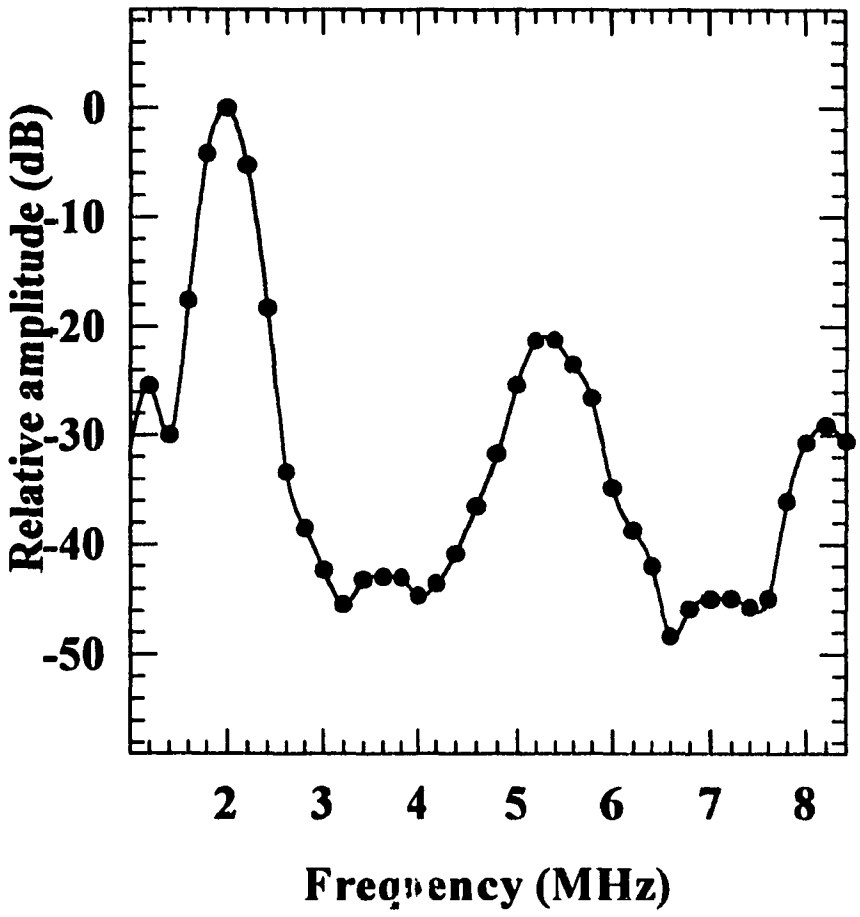

Figure 4.3 Frequency response measured on sample No. 1.

With the same transducer, different propagation modes may be excited at different frequencies. In Fig. 4.4 we can see that at 4.2 MHz, two different types of echoes (marked *A* and *S*, respectively) with different group velocities co-exist in the echo train, signal *A* being more clearly seen. Signal *S*, the one with a shorter delay, becomes more visible at 4.4 MHz, while signal *A* becomes less significant at this frequency. As the frequency

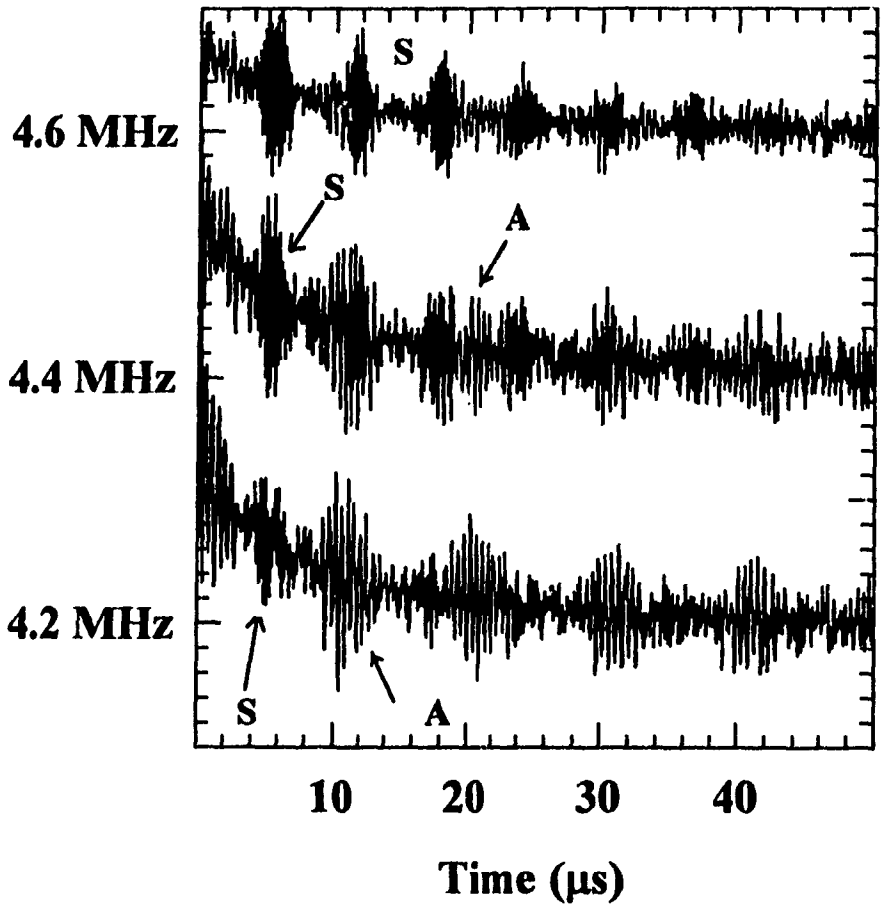

Figure 4.4 Time-delayed signals measured on sample No. 1.

changes to 4 6 MHz, signal *S* becomes dominant and signal *A* almost disappears.

Fig. 4.5 presents the frequency dependence of the group velocities of the circumferential waves measured of sample No.1, derived from the measured time delays at frequencies between 0.2 and 6.0 MHz with an interval of 0.2 MHz. It is clearly seen that the waves are dispersive and two different modes have been excited. The calculated group

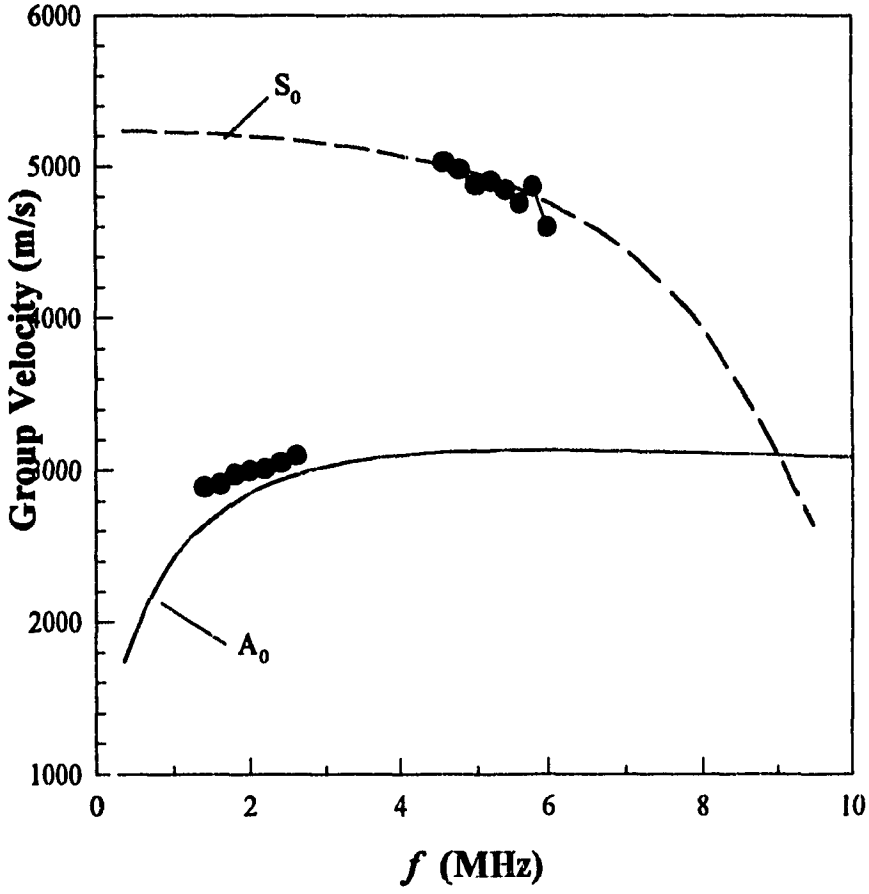

Figure. 4.5 Frequecy dependence of the group velocity measured on sample No. 1 for the circumferential waves (filled circle) and on Sample No. 2 for the axial waves (hollow circle), and the theoretical group velocity curves of a stainless steel plate (solid and dashed lines) with a thickness of 0.254 mm.

velocity curves of the lowest antisymmetric mode A_0 and the lowest symmetric mode S_0 for a stainless steel plate with a thickness of 0.254 mm are also included in Fig. 4.5 for comparison. The results suggest that two plate-like circumferential tube modes have been excited near the frequencies 2 MHz and 5.4 MHz, respectively, and that for a tube with $h/a \approx 1/20$ and $h \approx \lambda/4$, where $\lambda = 1$ *mm*, the circumferential waves are already very close to their corresponding plate waves. A numerical computation of the dispersion curves for a tube determined by Eq. (2.21) in Chapter 2 is requred for a more

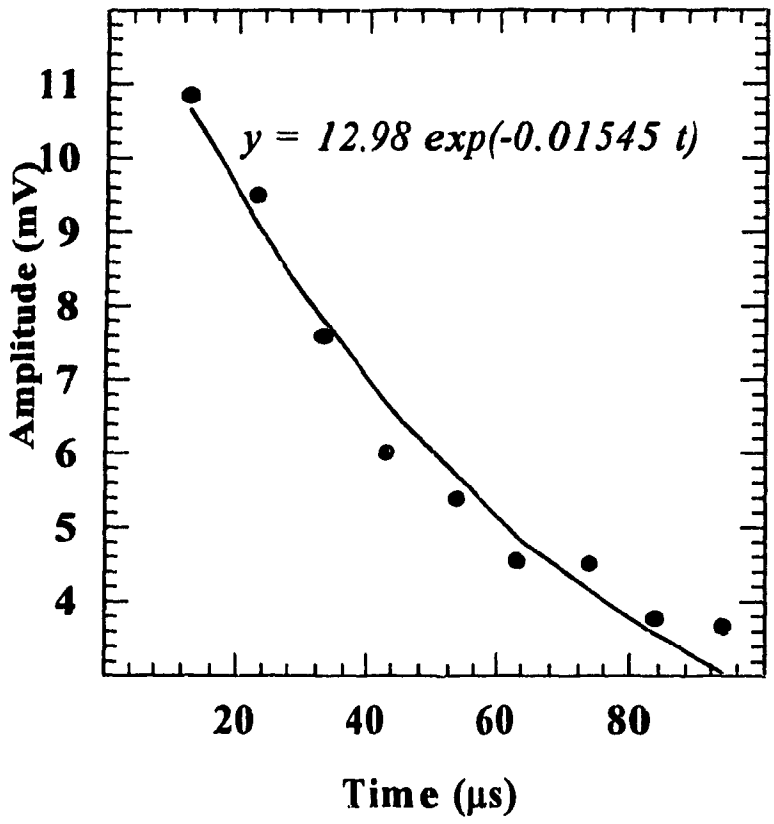

Figure 4.6 Attenuation curve for the circumferential tube wave in sample No. 1

definitive mode assignment.

In Fig. 4.2, we have also observed that in the echo train the amplitude of the signals decreases slowly, which indicates a low attenuation in the PZT coated stainless tube at the center frequency 2 MHz. A calculated attenuation curve fitted from the measured data of sample No. 1 at 2 MHz. is given in Fig. 4.6. An attenuation coefficient of 0.01545 neper / micro second or 44.8 dB / meter was derived. For a longitudinal bulk wave in mild steel, the reported attenuation coefficient is about 29 dB / meter [100]. This

means the coated PZT film did not increase substantially the attenuation in the stainless steal tube, which suggests that the film quality is reasonable.

while strong acoustic signals with good signal-to-noise ratio were observed along the circumferential direction on sample No. 1, the signals obtained for the axial waves on sample No. 2 were weaker. Apart from the fact that along the circumferential direction waves departing from both directions of the IDT have contribution to the received signals, there could be other causes such as the quality of the PZT films and their electric poling.

Fig. 4.7, 4.8 (a) and 4.9 (a) show the time-delayed signals measured at 1.74 MHz along the axial direction of a PZT-coated stainless steel tube (sample No 2) with the same wall thickness (0.254 mm) and outer diameter (9.6 mm) as those of sample No.1. The waveform of the signal transmitted from IDT 1 and received by IDT 2 is shown in Fig. 4.7. In Fig. 4.8 (a) , the major echo marked S_F represents the acoustic signal generated by IDT 1 and reflected from the farther end F of the tube to IDT 2, and echo S_N is the signal reflected from the nearer end N of the tube, respectively. The reason that the echo from the far end of the tube is stronger than that from the near end is not well understood but is probably due to the odd tube-end (see Fig 4.8 (b)) which may focus the acoustic energy. There could also be a transformation of the excited acoustic mode, when reflected at the tube ends, to different modes which could be more efficiently reconverted into electrical signals by the IDT. This might lead to the phenomenon that the reflected signals are stronger than the directly transmitted one.

We also performed the measurement on sample No.2 with a reflection geometry, where each of the two IDTs was used as the transmitter and receiver. In Fig 4.9 (a), the major echoes marked (1) and (2) were excited by transducer 1 and 2, reflected at the far

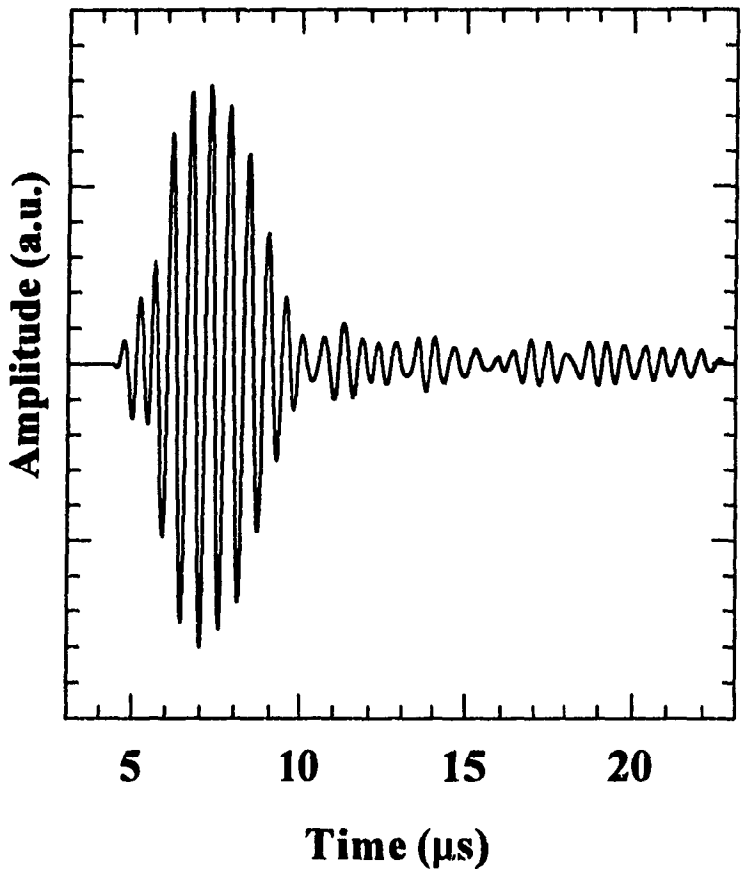

Figure 4.7 Waveform of the acoustic signal excited by IDT 1 and received by IDT 2 along the axial direction of a PZT-coated stainless steel tube.

end of the tube and then received by IDT 1 and IDT 2, respectively. The difference between the time delays of the echoes received by the two IDTs is estimated to be 10.8 μs, corresponding to a group velocity of about 3300 m / s, at which this acoustic signal traveled twice the center-to-center distance between the two IDTs. This low group velocity indicates that these reflected waves may be either the lowest axially symmetric mode L_{01}, which corresponds to the lowest antisymmetric plate mode, or the lowest flexural tube mode F_{11} [76].

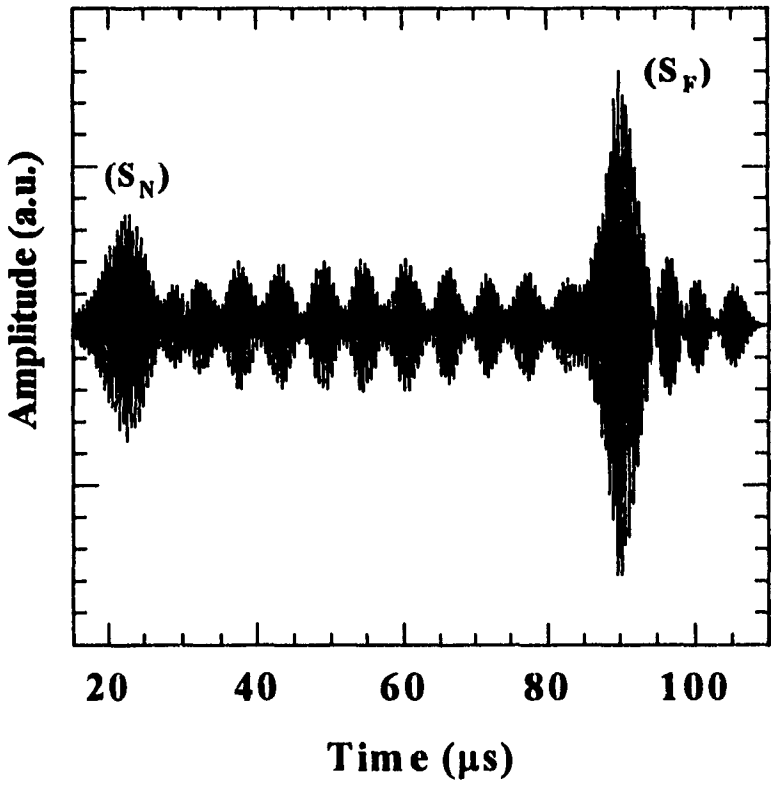

(a)

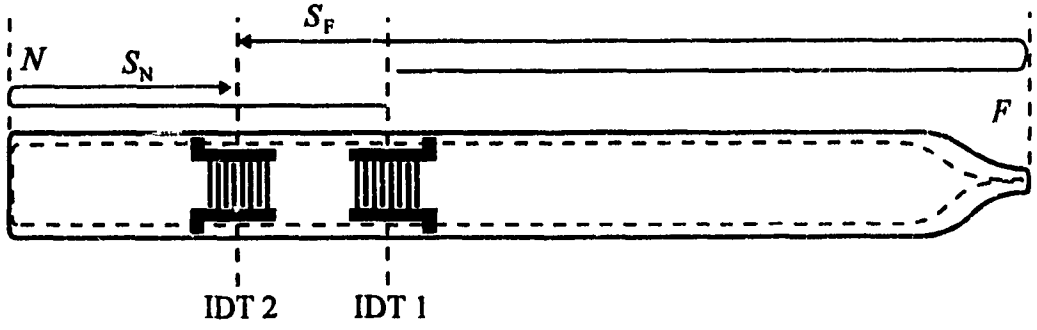

(b)

Figure 4.8 (a) Signals generated by IDT 1, reflected from the tube ends and then received by IDT 2 observed on sample No. 2 along the axial direction. (b) Illustration of the traveling paths of the echoes shown in (a).

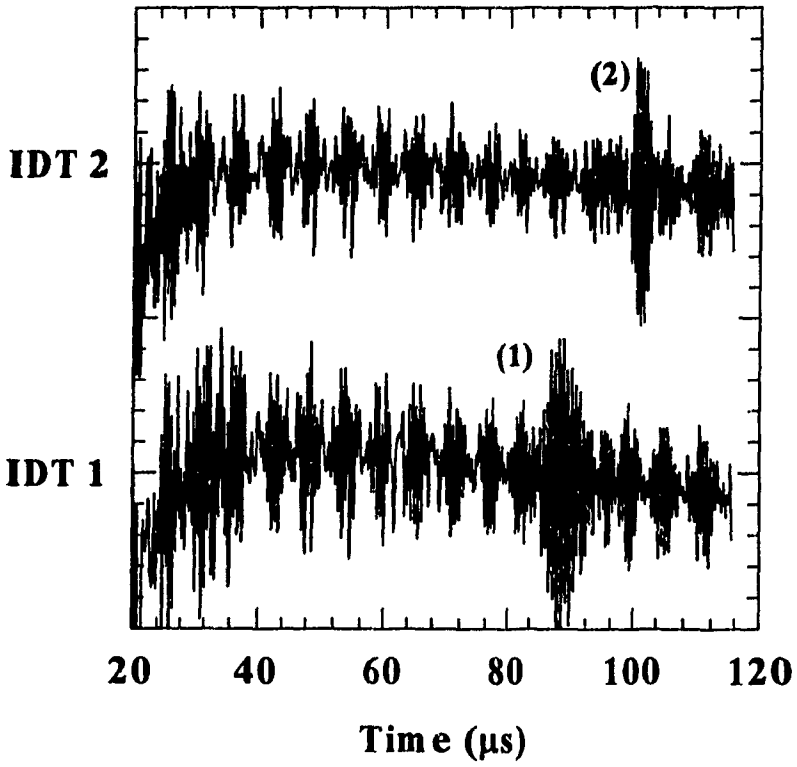

(a)

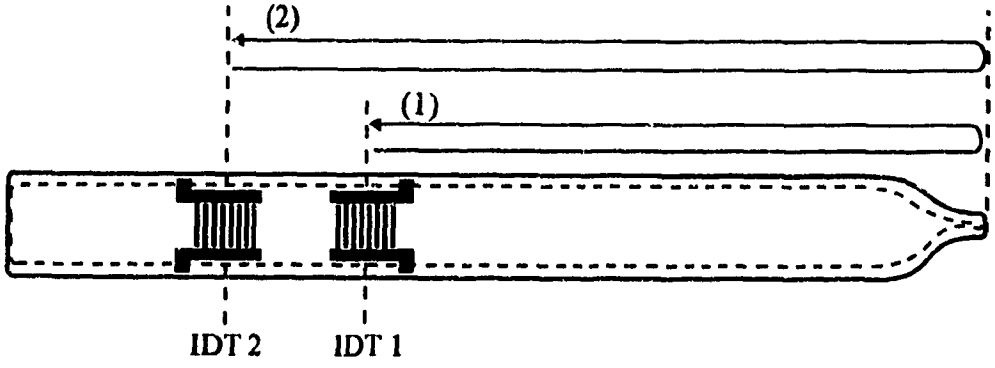

(b)

Figure 4.9 (a) Signals generated by one IDT (the upper one by IDT 1 and lower one by IDT 2, respectively), reflected from the far end of the tube, and received by the same IDT, observed on sample No. 2. (b) Illustration of the traveling paths of the echoes in (a).

Due to the mass loading and finite thickness of the IDT, reflection of the excited acoustic waves by the IDT fingers may occur [97,98]. The minor echo trains observed in Fig. 4.8 and Fig. 4.9 are the acoustic signals reflected by the IDTs, bouncing back and forth between the transmitter and the receiver. Since the waves reflected by the IDT fingers are all in phase, the resulted signals could be pronounced as observed. The time delay between two of the minor echoes is about 5.7 μs, from which a group velocity of 6300 m/s is derived. This very high group velocity value can not be interpreted by the curves given in Fig. 4.5. Theoretical dispersion curves for the axial tube waves are required and the non-axially symmetric modes should also be taken into account. Qualitatively, since waves with polarizations perpendicular to the axial direction would hardly be reflected by the IDT fingers the tube surface, the observed minor echoes could be resulted only from the reflection of the extensional waves rather than flexural waves, even though the group velocity of a non-axially symmetric mode could be as high as that of an extensional one [76].

The above two modes of very different group velocity observed at the same frequency also suggest that a mode conversion might have happened during the reflection at the tube end *F*.

When the *inner* side of the tubes, either for sample No.1 or No. 2, was wetted with water, the acoustic signals were substantially attenuated. This also indicates that the waves excited in these thin-walled tubes are plate-like, and sensing with the inner side is possible.

Both real and imaginary parts of the input impedance of the IDTs on sample No. 1 measured at the fundamental frequency around 2 MHz is 12 Ω - j12 Ω. The insertion loss mechanism includes the electromechanical coupling and propagation loss. At the fundamental frequency the latter loss is much smaller than the former one.

To investigate the effect of liquid loading in the tube wave device, we filled the tube with water. Fig. 4.10 shows signals of the circumferential waves observed on sample No. 1 before and after being filled with water inside. We can see that the amplitude of the signals and the time delays are obviously different in these two cases. It can be seen that when loaded with water, the attenuated successive echoes is still significant, indicating that sensing in a liquid phase using this circumferential mode is possible. From the results a decrease of the group velocity about 25 % is estimated. This large liquid-loading effect on the group velocity of this A_0-like circumferential mode in the tube makes it possible to use this type of device, for example, to sense liquids with different densities. Theoretical study of the liquid-loading mechanism in tubes and further experiments are in progress.

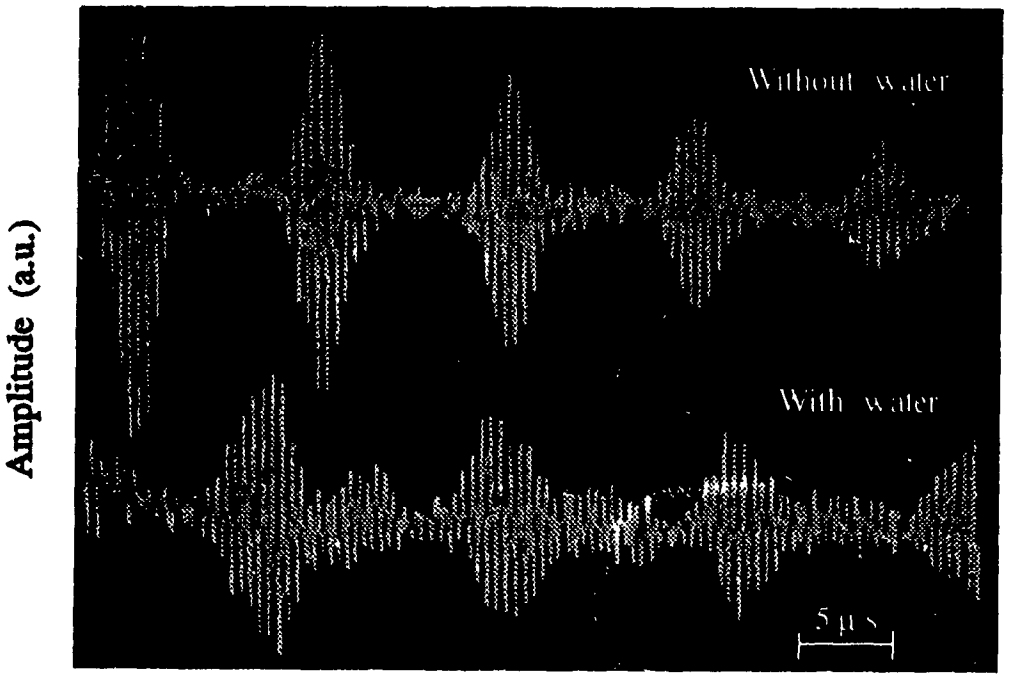

Figure 4.10 Signals of the circumferential waves observed on sample No. 1 before (the upper echo train) and after (the lower echo train) being filled with water inside.

CHAPTER 5: CONCLUSIONS

Ultrasonic thin-walled tube devices for sensor considerations were theoretically and experimentally investigated. We have shown that similar to ultrasonic plate wave sensors, these configurations provide advantages of separating the sensing medium from the sensor electronics and of high mass sensitivity for several modes provided that the tube wall thickness h is very thin ($h << \lambda$, where λ is the acoustic wavelength). A further advantage is that the inner side of the tube can be used as a natural and smooth chamber or flow channel of the gases or liquid to be monitored, since the construction of a chamber or flow channel for use in sensors such as bulk (BAW), surface (SAW), plate (PAW) and thin rod sensors has been a practical concern due to its large size and the possible turbulence caused by the corners existed in the chamber or channel.

In order to reach an integrated sensor configuration, a sol-gel process for the fabrication of thin piezoelectric lead zirconate titanate (PZT) films coated coaxially on stainless steel tubes was developed. This sol-gel process of low cost is suitable for the film fabrication of large areas and on complex shapes. Crack free PZT films with thicknesses up to several microns and coating lengths more than several centimeters have been achieved. So far, the coating length has been limited by our experimental apparatus. Interdigital transducers (IDT), which excited the ultrasonic waves and reconvert them into electrical signals, were fabricated as the transmitter and receiver on the curved tube surfaces. Each IDT had 8 finger pairs (8 mm in length) and a 6 mm aperture. The width of each electrode and gap was 250 μm. Along the axial direction a delay line configuration was adopted to measure the velocity of the acoustic modes and the distance between the center of the transmitting and receiving IDT's was 18 mm. Along the circumferential direction a resonator or delay line geometry was made with a single IDT. In addition to stainless steel tubes, PZT films have also been successfully deposited and poled on aluminum tubes.

Experimental measurements along the circumferential direction of stainless steel tubes have been performed between 0.2 to 8.4 MHz. The results show that two modes with different dispersion have been observed. Both real and imaginary parts of the IDT's input impedance at the fundamental frequency is around 12 Ω - j12 Ω. The insertion loss mechanism includes the electromechanical coupling and propagation loss. At the fundamental frequency around 2 MHz the latter loss is much smaller than the former one. Along the circumferential direction the signal was stronger than that along the axial direction. Apart from the fact that along the circumferential direction waves departing from both direction of the IDT have contribution to the received signals, there could also be other causes such as the quality of the PZT films and their electric poling. The effect of liquid loading in the tube device on the circumferential mode was also investigated. The results suggest that a sensing in liquid phase is possible using this mode.

We have also theoretically analyzed the wave propagation characteristics and mass sensitivity of different modes propagating in a tube device with a density of ρ, and a and b as the inner and outer radius respectively. We show that the mass sensitivity for the lowest axially symmetric mode is $-1/[\rho h\ (1+ a/b)]$ and that for the lowest torsional mode is $-1/[\rho h\ (1+ a/b)(1+ a^2/b^2)]$, respectively provided that the mass loading layer is deposited at the inner wall of the tube. These results indicate that high mass sensitivity can be achieved by using thin wall (small h) tubes and makes these devices excellent sensor candidates.

REFERENCES

1. J.B. Miller and D.I. Bolef, "Acoustic wave analysis of the operation of quartz crystal film-thickness monitors," J. Appl. Phys., vol.39, pp.5815-5816, 1968.
2. D.L. Hammond and A. Benjaminson, "The crystal resonator, a digital transducer," IEEE Spectrum, vol.6, pp.53-60, 1969.
3. C.S. Lu and O. Lewis, "Investigation of film-thickness determination by oscillating quartz resonators with large mass load," J. Appl. Phys., vol.43, p. 4385, 1972.
4. C.S. Lu, "Mass determination with piezoelectric quartz crystal resonators," J. Vac. Sci. Technol., 12, p. 578-583, 1975
5. D. Hauden, "Miniaturized bulk and surface acoustic wave quartz oscillators used as sensors," IEEE Trans. Ultrason., Ferroelectrics, Freq. Control, vol.UFFC-34, pp.253-258, 1987
6. H. Ito, "Balanced adsorption quartz hygrometer," IEEE Trans. Ultrason. Ferroelect. and Freq. Control, vol.UFFC-34, pp.136-141, 1987.
7. T. Nakamoto and T. Moriizumi, "Odor sensor using quartz-resonator array and neural-network pattern recognition," Proc. IEEE Ultrasonics Symp., 88CH2578-3, pp.613-616, 1988.
8. F. Josse, Z.A. Shana, D.E. Radtke, and D.T. Haworth, "Analysis of piezoelectric bulk-acoustic-wave resonators as detectors in viscous conductive liquids," IEEE Trans. Ultrason., Ferroelectrics, Freq. Control, vol.UFFC-37, pp.359-368, 1990
9. M. Thompson, A.L. Kipling, W.C. Duncan-Hewitt, L.V. Rajakovic, and B.A. Cavic-Vlasak, " Analyst, vol.116, pp.881-890, 1991.
10. G.J. Price and J. M Buley, "Quartz crystal microbalance apparatus for studying interactions of solvents with thin polymer films," Progress in Organic Coatings, vol.19, pp.265-274, 1991.

11. C. Gabrielli, M. Keddam, and R. Torresi, "Calibration of the electrochemical quartz crystal microbalance," J. Electrochem. Soc., vol.138, pp.2657-2660, 1991.

12. J.T. Kucera, J.D. Perkins, K. Uwai, J.M. Graybeal and T.P. Orlando, "Detection of ozone using a silver coated quartz crystal rate monitor," Rev. Sci. Instrum., vol.62, pp.1630-1632, 1991.

13. S.J. Martin, V.E. Granstaff, and G.C. Frye, "Characterization of a quartz crystal microbalance with simultaneous mass and liquid loading," Anal. Chem. vol.63, pp.2272-2281, 1991.

14. S.J. Martin, G.C. Frye, A.J. Ricco, and S.D. Senturia, "Effect of surface roughness on the response of thickness-shear mode resonators in liquids," Anal. Chem., vol.65, pp.2910-2922, 1993.

15. T.M. Reeder and D.E. Cullen, "Surface acoustic wave pressure and temperature sensors," Proc. of the IEEE, vol.64, pp.754-756, 1976.

16. P. Das, C. Lanzl, and H.F. Tiersten, "A pressure sensing acoustic wave resonator," Proc. IEEE Ultrasonics Symp., pp.306-308, 1976.

17. H. Wohltjen and R. Dessy, "Surface acoustic wave probe for chemical analysis. I. Introduction and instrument description, II. Gas chromatography detector, III. Thermomechanical polymer analyzer," Anal. Chem., vol.51, pp.1458-1478. 1979.

18. D. Hauden, G. Jaillet, and R. Coquerel, "Temperature sensor using SAW delay line," Proc. IEEE Ultrasonics Symp., 81CH1689-9, p. 148-151, 1981.

19. H. Wohltjen, "Mechanism of operation and design considerations for surface acoustic wave device vapour sensors," Sensors and Actuators," vol.5, pp.307-325, 1984

20. S.J. Martin, K.S. Schweizer, S.S. Schwartz, and R.L. Gunshor, "Vapor sensing by means of a ZnO-on-Si surface acoustic wave resonator, Proc. IEEE Ultrasonics Symp., 84CH2112-1, pp.207-212, 1984.

21. S.G. Joshi, "Surface acoustic wave voltage sensor with improved sensitivity," Proc. of the IEEE, vol.72, pp.1418-1419, 1984.

22. R.M. White, "Surface acoustic wave sensors," Proc. IEEE Ultrasonics Symp., pp.490-494, 1985.

23. A. Venema, E. Nieuwkoop, M.J. Vellekoop, M.S. Nieuwenhuizen, and A.W. Barendsz, "Design aspects of SAW gas sensors," Sensors and Actuators, vol.10, pp.47-64, 1986

24. D.S. Ballantine, S.L. Rose, J.W. Grate, and H. Wohltjen, "Correlation of surface acoustic wave device coating responses with solubility properties and chemical structure using pattern recognition," Analytical Chemistry, vol.58, pp.3058-3066, 1986.

25. H. Wohltjen, A.W. Snow, W.R. Barger, and D.S. Ballantine, "Trace chemical vapor detection using SAW delay line oscillators," IEEE Trans. Ultrason., Ferroelectrics, Freq. Control, vol.UFFC-34, pp.172-178, 1987.

26. S.J. Martin, A.J. Ricco, D.S. Ginley, and T.E. Zipperian, "Isothermal measurements and thermal desorption of organic vapors using SAW devices," IEEE Trans. Ultrason., Ferroelectrics, Freq. Control, vol UFFC-34, pp.143-147, 1987.

27. J.F. Vetelino, R.K. Lade, and R.S. Falconer, "Hydrogen sulfide surface acoustic wave gas detector," IEEE Trans. Ultrason., Ferroelectrics, Freq. Control, UFFC-34, pp.156-161, 1987.

28. A. Venema, E. Nieuwkoop, M.J. Vellekoop, W.J. Ghijsen, A.W. Barendsz, and M.S. Nieuwenhuizen, "NO gas-concentration measurement with a SAW-chemosensor," IEEE Trans. Ultrason., Ferroelectrics, Freq. Control, vol.UFFC-34, pp.148-155, 1987.

29. M.E. Motamedi, "Acoustic accelerometers," IEEE Trans. Ultrason., Ferroelectrics, Freq. Control, vol.UFFC-34, pp.237-242, 1987.

30. V.V. Varadan, Y.R. Roh, and V.K. Varadan, "Local/Global SAW sensors for turbulence," Proc. IEEE Ultrasonics Symp., pp.591-594, 1989.

31. S.J. Martin and G.C. Frye, "Surface acoustic wave response to changes in viscoelastic film properties," Appl. Phys. Lett., vol.57, pp.1867-1869, 1990.

32. W.M. Heckl, F.M. Marassi, K.M. R. Kallury, D.C. Stone and M. Thompson, "Surface acoustic wave sensor response and molecular modeling: selective binding of nitrobenzene derivatives to (aminopropyl) triethoxysilane," Anal. Chem., Vol.62, pp.32-37, 1990.

33. T. Nomura and T. Yasuda, "Measurement of velocity and viscosity of liquid using surface acoustic wave delay line," Japanese J. Appl. Phys. Part.1 - Regular Papers & Short Notes, vol.29, p.p.140-143, 1990.

34. M. Viens and J.D.N. Cheeke, "Highly sensitive temperature sensor using SAW resonator oscillator," Sensors and Actuators A, 25, pp.209-211, 1990.

35. J.W Grate and M. Klusty, "Surface acoustic wave vapor sensors based on resonator devices," Analytical Chemistry, vol.63, pp.1719-1727, 1991.

36. G.C. Frye, S.J. Martin, R.W. Cernosek, K.B. Pfeifer, and J.S. Anderson, "Portable acoustic wave sensor systems," Proc. IEEE Ultrasonics Symp., 91CH3079-1, pp.311-316, 1991.

37. R.L. Baer, C.A. Floy, M. Tom-Moy and D.S. Solomon, "STW chemical sensors," Proc. 1992 IEEE Ultrasonics Symposium, pp.293-298, 1992.

38. G. Kovacs and A. Venema, "Theoretical comparison of sensitivities of acoustic shear wave modes for (bio)chemical sensing in liquids," Appl. Phys. Lett., vol.61, pp.639-641, 1992.

39. E. Gizei, A.C. Stevenson, N.J. Goddard and C.R. Lowe, "A novel Love-plate acoustic sensor utilizing polymer overlayers," IEEE Transactions on Ultras. Ferroele. Freq. Contr., Vol.UFFC-39, pp.657-659, 1992.

40. J. Kondoh and S. Shiokawa, "SH-SAW taste sensor based on acoustoelectric interaction," Proc. Ultrasonics Symp., pp., 1993.

41. Z. Wang, J.D.N. Cheeke and C.K. Jen, "Sensitivity analysis for Love mode acoustic gravimetric sensors," Appl. Phys. Lett., vol.64, pp.2940-2942, May 1994.

42. R.M. White, P.J. Wicher, S.W. Wenzel and E.T. Zellers, "Plate mode ultrasonic oscillator sensors," IEEE Trans. Ultrason. Ferroelect. and Freq. Control, Vol.UFFC-34, pp.163-171, 1987.

43. J. Hou and H.Van de Vaart, "Mass sensitivity of plate modes in surface acoustic wave devices and their potential as chemical sensors," Proc. Ultrasonics Symp., pp.573-578, 1987.

44. T.M. Niemczyk, S.J. Martin, G.C. Frye, and A.J. Ricco, "Acoustoelectric interaction of plate modes with solutions," J. Appl. Phys., vol.64, pp.5002-5008, 1988.

45. S.W. Wenzel and R.M. White, "A multisensor employing an ultrasonic Lamb-wave oscillator," IEEE Trans. Electron Devices, vol.35, pp.735-743, 1988.

46. S.W. Wenzel and R.M. White, "Analytical comparison of the sensitivities of bulk-wave, surface-wave, and flexural plate-wave ultrasonic gravimetric sensors," Appl. Phys. Lett., vol.54, pp.1976-1978, 1989.

47. S.J. Martin, A.J. Ricco, T.M. Niemzyk and G.C. Grye, "Characterization of SH acoustic plate mode liquid sensor," Sensors and Actuators, vol.22, pp.253-268, 1989.

48. B.A. Martin, S.W. Wenzel, R.M. White, "Viscosity and density sensing with ultrasonic plate waves, Sensors and Actuators, A21-A23, pp.704-708, 1990.

49. Y. Jin and S.G. Joshi, "Coupling of interdigital transducer to ultrasonic Lamb waves," Appl. Phys. Lett., vol.58, pp.1830-1832, 1991.

50. M. Hoummady and F. Bastien, "Acoustic wave viscometer," Rev. of Scientific Instruments, vol.62, pp.1999-2003, 1991.

51. J.W. Grate, S.W., Wenzel, and R.M. White, "Flexural plate wave devices for chemical analysis," Anal. Chem., vol.63, pp.1552-1561, 1991

52. F. Josse and Z.A. Shana, "Electrical surface perturbation of a piezoelectric acoustic plate mode by conductive liquid loading," IEEE Trans. Ultrason., Ferroelectrics, Freq. Control, vol.UFFC-39, pp.512-518, 1992.

53. Z. Wang, C.K. Jen and J.D.N. Cheeke, "Mass sensitivity of two-layer shear horizontal plate wave sensors," Ultrasonics, vol.32, pp.209-215, 1994.

54. Z. Wang, C.K. Jen and J.D.N. Cheeke, "Mass sensitivity of two-layer sagittal plane plate wave sensors," Ultrasonics, vol.32, pp.201-208, 1994.

55. C.K. Jen, J.E.B. Oliveira, J.C.H. Yu, J.D. Dai and J.F. Bussiere, "Analysis of thin rod flexural acoustic wave sensors," Applied Physics Lett., vol.56, pp.2183-2185, 1990.

56. Z. Wang, J.D.N. Cheeke and C.K. Jen, "Unified approach to analyze mass sensitivities of acoustic gravimetric sensors," Elect. Lett., vol.26, pp.1511-1512, 1990.

57. C.K. Jen, J.D. Dai, J.C.H. Yu, Z. Wang and J.D.N. Cheeke, "Analysis of thin rod flexural acoustic wave gravimetric sensors immersed in liquid," IEEE Trans. Ultrason., Ferroelectrics and Freq. Control, vol. 38, pp.312-314, 1991.

58. Z. Wang, M. Viens, C.K. Jen, J.D.N. Cheeke and Y. Liu, "Thin rod acoustic wave gravimetric sensors," Sensors and Materials, vol.3, pp.159-171, 1992.

59. P.C.H. Li, D.C. Stone, and M. Thompson, "Flexural thin-rod acoustic wave devices as chemical sensors," vol.65, pp. 2177-2180, 1993.

60. M. Viens, P. Li, Z. Wang, C.K. Jen, M. Thompson and J.D.N. Cheeke, "Gravimetric response of thin rod acoustic wave sensors," Proc. of IEEE Ultrasonics Symp. pp.359-364, 1993.

61. J.W. Grate, R.A. McGill, and M.H. Abraham, "Chemically selective polymer coatings for acoustic vapor sensors and array," Proc. IEEE Ultrasonics Symp., 92CH3118-7, pp.275-279, 1992.

62. A.E.H. Love, *A Treatise on the Mathematical Theory of Elasticity*, (Cambridge University Press Warehouse, 1893, 2nd edit.), Chap.16, pp.115-123.

63. R.M. Cooper and P.M. Maghdi, "Propagation of elastic waves in cylindrical shells, including the effects of transverse shear and rotary inertia," J. Acoust. Soc. Am., vol.28, pp.56-63, 1956.

64. G. Herrmann and I. Mirsky, "Three-dimensional and shell-theory analysis of axially symmetric motions of cylinders," J. Appl. Mech., vol.23, pp.563-568, 1956.

65. G. Herrmann and I. Mirsky, "Axially symmetric motions of thick cylindrical shells," J. Appl. Mech., vol.25, pp.97-102, 1958.

66. P.M. Maghdi and R.M. Cooper, "Propagation of nonaxially symmetric waves in elastic cylindrical shells," J. Acoust. Soc. Am., vol.29, pp.1365-73, 1957.

67. D.C. Gazis, "Exact analysis of the plane-strain vibrations of thick-walled hollow cylinders," J. Acoust. Soc. Am., vol. 30, pp.786-794, 1958.

68. D.C. Gazis, "Three-dimensional investigation of the propagation of waves in hollow circular cylinders. I. analytical foundation. II. numerical results," J. Acoust. Soc. Am., vol.31, pp.568-578, 1959.

69. J.E. Greenspon, "Vibration of thick-walled cylindrical shell - comparison of the exact theory with approximate theories," J. Acoust. Soc. Am. vol. 32, pp.571-578, 1960.

70. J.E. Greenspon, "Vibrations of thick and thin cylindrical shells surrounded by water," J. Acoust. Soc. Am. vol.33, pp.1321-1328, 1961.

71. C.R. Fuller, and F.J. Fahy, "Characteristics of wave propagation and energy distributions in cylindrical elastic shells filled with fluid," J. Sound Vib., vol.81, pp. 501-518, 1982

72. B.K. Sinha, T.J. Plona, S. Kostek and S.K. Chang, "Axisymmetric wave propagation in fluid-loaded cylindrical shells. I: Theory," J. Acoust. Soc. Am., vol.92, pp.1132-1143, 1992.

73. T.J. Plona, B.K. Sinha, S. Kostek and S.K. Chang, "Axisymmetric wave propagation in fluid-loaded cylindrical shells. II: Theory versus experiment," J. Acoust. Soc. Am., vol.92, pp.1144-1155, 1992.

74. W. Mohr and P. Höller, "On inspection of thin-walled tubes for transverse and longitudinal flaw by guided ultrasonic waves," IEEE Trans. Sonics and Ultrasonics, SU-23, pp.369-374, 1976.

75. M.G. Silk and K.F. Bainton, "The propagation in metal tubing of ultrasonic wave modes equivalent to lamb waves," Ultrasonics, vol. 7, pp.11-19 1979.

76. N.C. Nicholson and W.N. McDicken, "Mode propagation of ultrasound in hollow wave guides," Ultrasonics, vol.29, pp.441-416, 1991.

77. I.A. Viktorov and O.M. Zubova, "Normal plate modes in a solid cylindrical layer," Soviet Physics-Acoustics, vol.9, pp.15-17, 1963.

78. H.I. Epstein, "Circumferential waves in a composite circular cylinder," J. Sound Vib., vol.48, pp.57-71 1976.

79. I.A. Viktorov, "Ultrasonic Lamb waves (review)," Soviet Physics-Acoustics, vol.11, pp.1-14, 1965.

80. B. Jaffe, W.R. Cooke and H. Jaffe, *Piezoelectric Ceramics*, Academic Press, New York (1971).

81. C.M. Cotell and K.S. Grabowski, "Novel materials application of pulsed laser deposition," MRS. Bull. vol. XVII, 44-53(1992)

82. C.J. Brinker and G.W. Scherer, *Sol Gel Science*, Academ. Press Inc., San Diego, CA, 1990.

83. K.D. Budd, S.K. Dey and D.A. Payne, "Sol gel processing of PbTiO3, PZT and PLZT thin films," Brit. Ceram. Proc., vol. 36, pp.107-121, 1985.

84. S.K. Dey, D.A. Payne and K.D. Budd, "Thin film ferroelectrics of PZT by sol-gel processing," IEEE Trans Ultrason. Ferroelectr. Freq. Contr. vol.35, pp.80-81, 1988.

85. G. Yi, Z. Wu and M. Sayer, "preparation of Pb(Zr,Ti)O3 thin films by sol gel processing: electrical, optical and electro-optic properties," J. Appl. Phys. vol.64, pp.2717-2724 1988.

86. G. Yi, Z. Wu, K. Sreenivas, M. Sayer, C.K. Jen and G. Perluzzo, "Ultrasonic experiments with lead zirconate titanate thin films fabricated by sol-gel processing," Elect. Lett., vol.25, pp.307-309, March 1989.

87. G. Yi, M. Sayer, Z. Wu, C.K. Jen and J.F. Bussiere, "Piezoelectric lead zirconate titanate coatings on metallic wires," Elect. Lett., vol.25, pp.907-908, July 1989.

88. G.Yi, M. Sayer, C.K. Jen, J.C.H. Yu and E.L. Adler, "Coaxil thin film transducers based on PZT," Proc. IEEE Ultrasonics Symp., pp.1231-1235, 1989.

89. M. Sayer, "Piezoelectric thin film devices," Proc. IEEE Ultrason. Symp. pp.595-603, 1991.

90. G. Yi nd M. Sayer, "Sol-gel processing of complex oxide films," Ceram. Bull., vol. 70, pp.1173-1179, 1991.

91. R.W. Jones, *Fundamental Principles of Sol-Gel Technology*, Ch.8, pp81, Inst. of Metals, London, 1989.

92. G. Yi, "Sol-gel process of PZT films," Ph.D. thesis, Ch.1, pp.23, Ch.5, pp. 140-142, Queen's Univ., 1993.

93. G. Yi, private communications.

94. H.I. Smith, *Surface Wave Devices*, ed. by H. Matthews, Ch. 4, pp. 165-217, John Wiley and Sons, New York, 1977.

95. Z. Wang, private communications.

96. M. Sayer, C.V.R. Vasant Kumar, D. Barrow, Li. Zou and D.T. Amm, "Integrated piezoelectric devices from thin film ferroelectrics," Mat. Res. Soc. Symp. Proc., vol. 243, pp.39-48, 1992.

97. G.W. Farnell, "Surface reflectors and resonators," Canadian Elec. Eng. J., vol. 1, pp.3-13, 1976.

98. D.-P. Chen and H.A. Haus, " Analysis of metal-strip SAW gratings and transducers," IEEE Trans. Sonics Ultrason., vol. SU-32, pp.395-408, 1985.

99. J. Krautkrämer and H. Krautkrämer, *Ultrasonic Testing of Materials*, pp. 576, Springer-Verlag, Berlin Heidelberg New York, 1990.

100. G.S. Kino, *Acoustic Waves: Devices, Imiging, and Aanalog Signal Processing*, pp. 551, Prince-Hall, Inc., New Jersey, 1986.